ISSN 1028-8546

Volume XIX, Number 3
Section: En
October, 2013

Azerbaijan Journal of Physics

Fizika

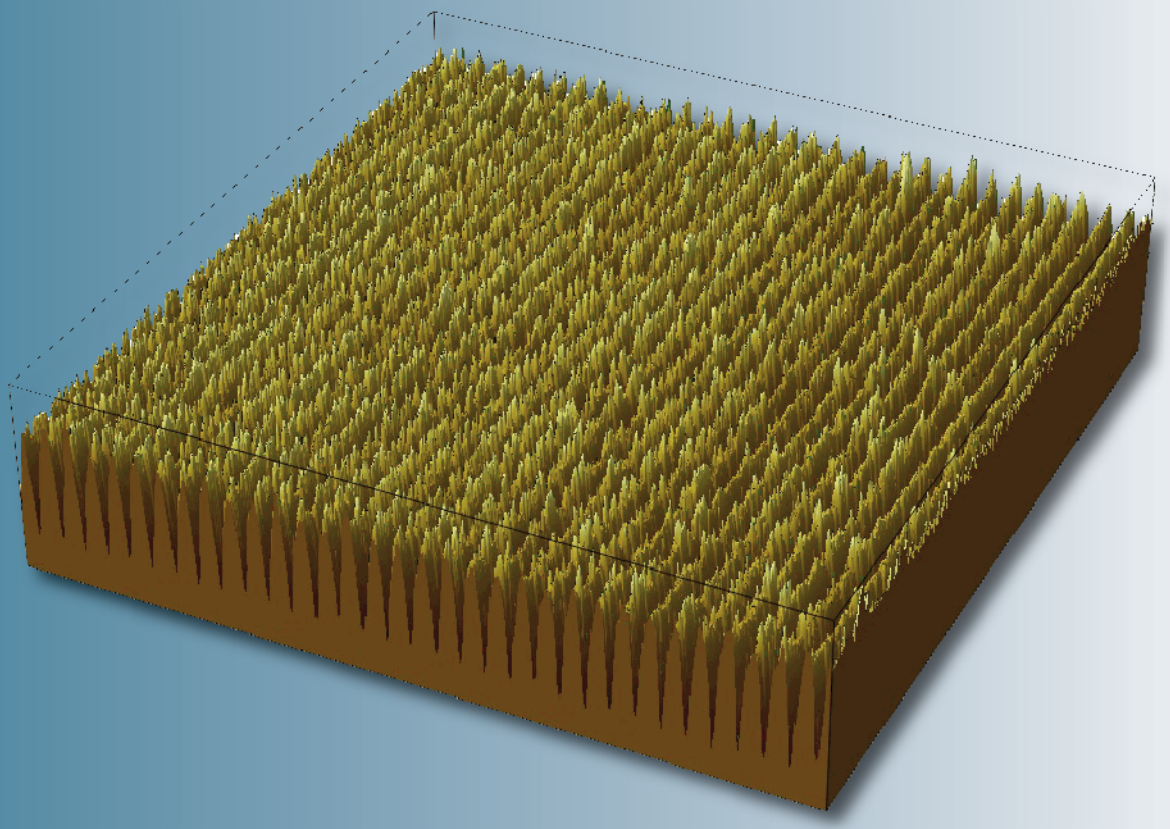

www.physics.gov.az

G.M. Abdullayev Institute of Physics
Azerbaijan National Academy of Sciences
Department of Physical, Mathematical and Technical Sciences

Published from 1995
Ministry of Press and Information
Of Azerbaijan Republic,
Registration number 402, 16.04.1997

ISSN 1028-8546
vol. XIX, Number 3, 2013
Series: En

Azerbaijan Journal of Physics

FIZIKA

G.M.Abdullayev Institute of Physics
Azerbaijan National Academy of Sciences
Department of Physical, Mathematical and Technical Sciences

PUBLISHING OFFICE

33 H.Javid ave, AZ-1143, Baku
ANAS, G.M.Abdullayev Institute of Physics

Tel.: (99412) 439-51-63, 439-32-23
Fax: (99412) 447-04-56
E-mail: jophphysics@gmail.com
Internet: www.physics.gov.az

It is authorized for printing: 04.10.2013

Published at "**SƏRQ-QƏRB**"
17 Ashug Alessger str., Baku
Typographer : Aziz Gulaliyev

Sent for printing on: __.__. 201_
Printing approved on: __.__. 201_
Physical binding:_____
Number of copies:_____200
Order:_____

SYNTHESIS OF CARBON NANOTUBES BY GASIFICATION OF PETROLEUM COKE

S.H. ABDULLAYEVA[1,2], N.N. MUSAYEVA[1,2*], R.B. JABBAROV[1,2], T. MATSUDA[3]
[1]G.M. Abdullayev Institute of Physics, Azerbaijan NAS, Baku, Azerbaijan
[2]Research & Development Center for Hi-Technologies, MCIT, Baku, Azerbaijan
[3]Osaka University, Japan
E-mail: nmusayeva@physics.ab.az

Carbon nanotubes have been synthesized by using petroleum coke (PC) as carbon source. Different positions of the PC in the reactor chamber and some other factors markedly increase quantity of the synthesized CNTs and lead to changing of their characteristics such as crystallinity, diameter, straight etc. confirmed by scanning electron microscope (SEM), transmission electron microscope (TEM) studies. The thickness of the Fe catalyst deposited on Si and SiO_2 substrates strongly influence to the quality, quantity and uniformity of the grown CNTs. Wet-coated thin films of $FeCl_2$ works well as catalyst, which can be profitable for mass production of CNTs

Keywords: Carbon nanotubes, petroleum coke, catalyst, byproduct.
PACS: 75.20. {g, 75.75.+a, 75.20.En, 75.30.Cr, 75.50.Bb

1. INTRODUCTION

Carbon nanotube, which is one of the allotrope of carbon, has been attracted worldwide after their discovery in 1991 by Iijma [1]. Carbon nanotubes have distinguishing properties like mechanical, thermal, electrical, etc. which make them useful in many fields starting from nanoelectronics to heavy industry.

CNTs can be classified into two main categories: single-walled carbon nanotubes (SWNTs) and multi-walled carbon nanotubes (MWNTs) [2]. It is of great interest to understand what factors control the nanotube sizes, number of shells, the helicity and the structure during synthesis; this is due to the fact that different atomic structure of the tubes may result in great changes in their properties [3-5].

In general, CNTs are synthesized by arc discharge [6], laser ablation [7], chemical vapor deposition (CVD) [8] and spray pyrolysis [9].

Although first two methods from above mentioned can produce high quality SWNTs, the available quantity from both arc discharge and laser ablation is limited.

CVD is more promising and cheaper method for synthesizing CNTs, for large scale production. Because good quality SWCNTs are quite expensive due to synthesis technologies. The other problem is to choose the suitable eco-friendly carbon source for synthesizing high quality CNTs with good parameters and low cost.

Many authors have been used different carbon sources, like cyclohexane, acetonitrile [10], benzene [11,12], xylene [13], alcohols [14] et.al. for synthesizing of both single and multiwall carbon nanotubes by CVD method.

In this work we demonstrate CNTs, synthesized by using byproduct of Caspian oil refiner.

Caspian oil is one of the high quality and light oil in the world. Oil in the Caspian has a long history - indeed it is one of the earliest oil production regions in the world, with Baku a major oil center in the second half of the 19th century and beyond. This Caspian Sea oil utilize as gasoline, Jet fuel, LPG, fuel oil, asphalt after refining.
We had an idea to use byproduct- Petroleum Coke (PC) of oil refiner as carbon source for synthesizing of CNTs. The refining process diagram is shown in fig.1.

To have knowledge about chemical contents of PC was carried out Gas chromatographic and Fluorescent X-ray analysis, which results are shown in fig 2.

We observed many aromatic hydrocarbons included in PC and impurities of oil are Cl, Al and S elements.

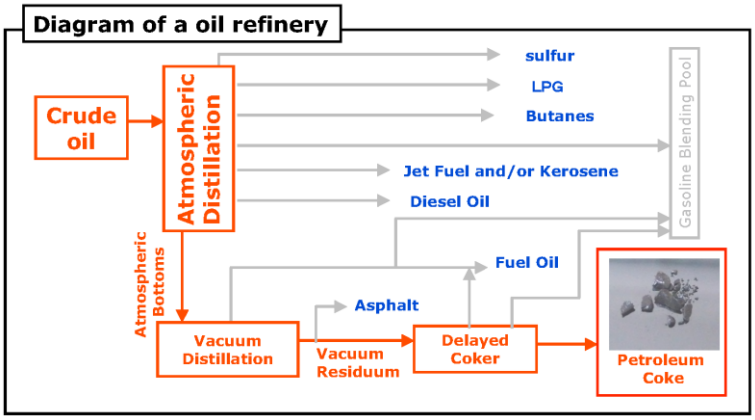

Fig. 1. Oil refining process.

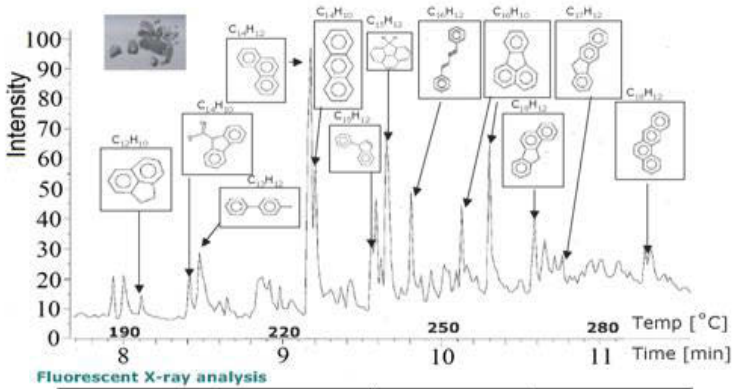

Fluorescent X-ray analysis

Element (> Na)	Cl	Al	S
Ratio[%]	50	27	23

Fig. 2. Gas chromatographic and Fluorescent X-ray analysis of the PC.

2. EXPERIMENTAL RESULTS AND DISCUSSION

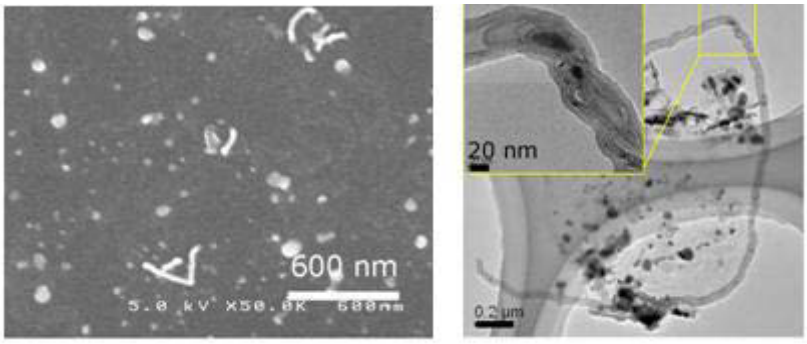

Fig 3. Gasification process under pure He (185 sccm); a) SEM observations; b) TEM observations

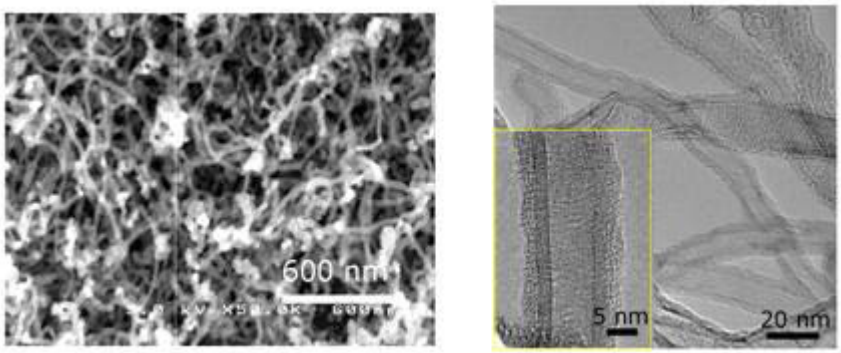

Fig. 4. Gasification process under He 105 sccm + H_2 80 sccm; a) SEM observations; b) TEM observations.

Very thin Fe film has been deposited on Si and SiO_2 substrates by RF sputtering technique. Fe small particles on the substrate used as catalyst for CNTs growth by gasification of PC – natural carbon source. PC has putted to the reactor, which is occupied by electric furnace. This electric furnace has tree zone of heating: heating zone of carbon source, vapor-phase transport zone, heating zone of catalyst. The vapor in the reactor is transported in 2 steps:

1. He gas 185 sccm;
2. He 105 sccm + H_2 80 sccm

Synthesized CNTs have been analyzed by Scanning electron microscope (SEM) HITACHI S-4500 and Transmission electron microscope TEM) JEOL SE-2500 It is observed that the 700 ^{0}C is optimal temperature to grow CNTs by our synthesis method.

There are also some cases, which can optimize the growth process:

a)H_2 is key

In first experiments we used only pure He (185 sccm) gas as a transporter. In this case is grown very little quantity of carbon nanotubes on Fe/SiO_2 substrate, as it is seen from SEM observations (fig.3 (a)) TEM observation show that the grown CNTs in this condition are bamboo like(fig.3 (b)).

In the next experiments have been used He 105 sccm + H_2 80 sccm, and we are obtained very much

quantity CNTs on Fe/SiO_2 substrate in the same conditions (furnace temperature and reaction time). It is observed that, synthesized CNTs by this condition are more straight (fig.4 a and b). In fact that the following changes are expected when H_2 presence in the reactor chamber:

- Enhance the dissociation of higher order of hydrocarbon molecules.
- Remove carbon atoms weakly bonded on the surface of CNTs.
- Prevent the deactivation of the catalyst.

The role of hydrogen in chemical vapor decomposition (CVD) of C_2H_4 for growth of carbon nanotubes (CNTs) was investigated by several authors, which reported that presence and quantity of hydrogen significantly influence to the structure of the grown CNTs (size, structure, morphology, or areal nanotube density) [15–22].

b) Heating procedure of cokes

The experiments show that the geometrical position of coke – as carbon source greatly influences to parameters of obtained CNTs. We have chosen three different positions for coke during the growth process: outside of the furnace; at edge of the furnace; inside of the furnace. All the positions have been shown in fig.5.

Fig. 5. PC positions in the reactor.

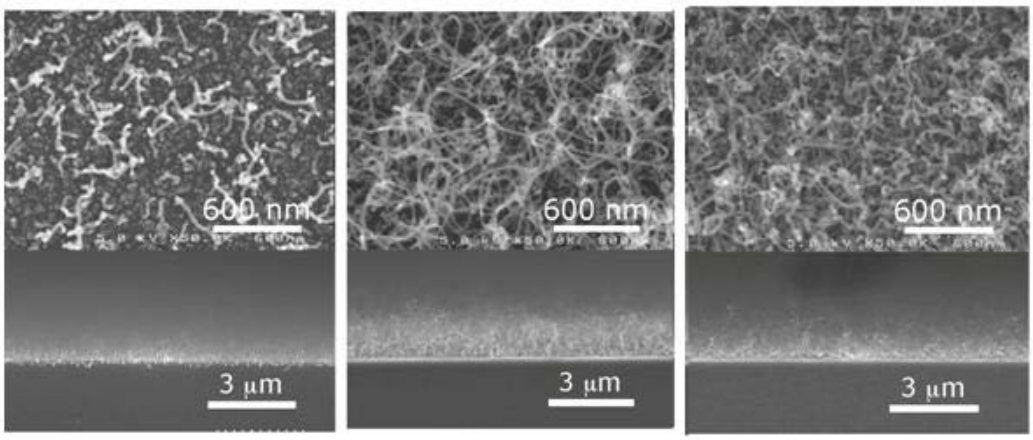

Fig.6. SEM observations of CNTs grown in cases PC is: a) outside of the furnace; b) at edge of the furnace; inside of the furnace

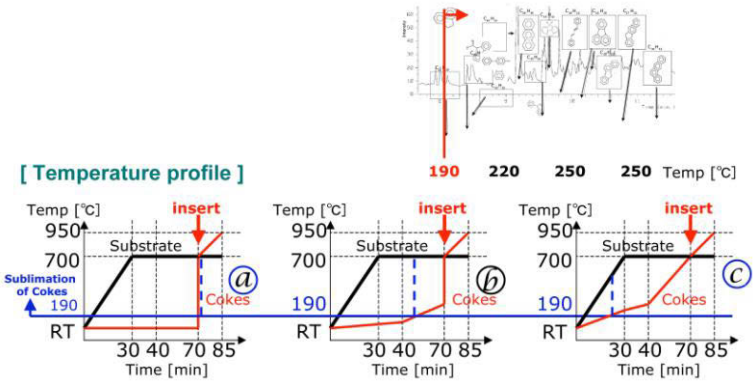

Fig. 7. Schematic illustration of the processes in the reactor depending of the PC position.

In the first position coke is not heated for a long time, while inside it evaporates very quickly at high temperatures. Fig. 6 shows SEM results of all cases. It is observed that, better result is obtained when coke is in edge of the furnace. This phenomenon can be explained schematically with the diagrams (Fig.7). In first case excess carbon was supplied in a short period and worked to deactivate the catalyst. When the coke is in edge of the furnace the moderate carbon was supplied after the substrate reached to 700 ˚C. The diagram shows that the carbon was supplied before the catalyst was activated in the case of coke was inside of furnace.

a) Role and thickness dependence of the catalyst

The catalyst (in this case a metal) is involved to control the kinetics of reactions such as decomposition of the precursor. It also acts as a geometric confinement for the forming CNT-structure. The catalyst can be located on a substrate or is delivered via the gas phase [23-25].

The correlation between prepatterned catalyst film thickness and carbon nanotube (CNT) growth by selective

area chemical vapor deposition (CVD) was studied using Fe, Co and Ni as catalysts [26,27].

But the specific role of the catalyst in the nanotube growth process is not clear. Several growth mechanisms have been proposed, among them those where growth is expected to take place at "base"[28] and "tip" [29] locations with respect to the nanotube, have received partial evidences from experimental and theoretical studies. The main difference between them is given by the behavior of the C-metal nanoparticle during the growth process.

In this work very thin Fe thin films were deposited on Si substrate by sputtering. Experiments show that when Fe layer thickness less than 1 nm, smallest and less quantity CNT s are grown on the substrate. Better result obtained when Fe thickness are between 1-2 nm (Fig.8). In this study, we used powders (control experiment) and wet coated 0.01% 40 µl (liquid) $FeCl_2$ as the catalyst to grow CNTs on quartz substrates. Both substrates putted in hot zone of the quarts reactor and growth temperature was 820°C. SEM shows top views of the samples (Fig.9). Thin and spinnable CNTs are grown on thin coated $FeCl_2$, while CNTs grown on $FeCl_2$ powder are thicker and longer.

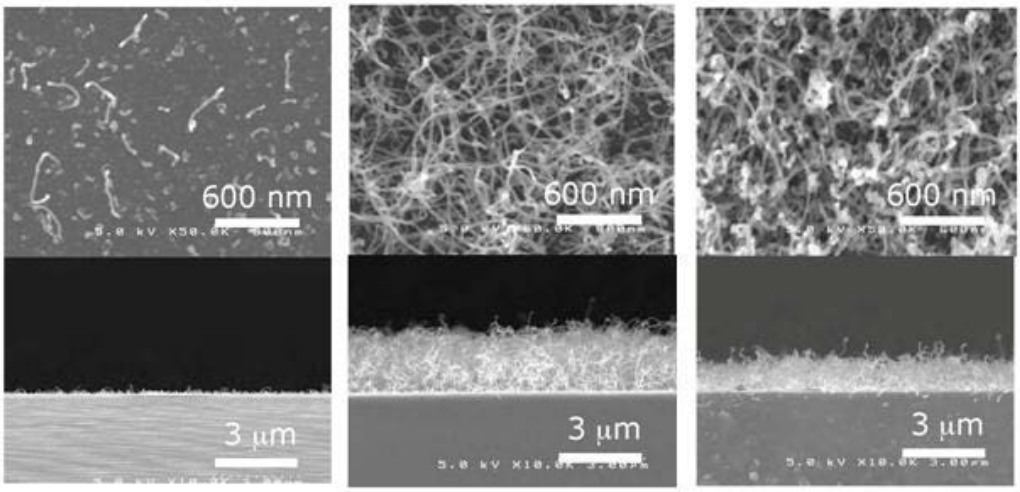

Fig. 8. SEM observations of CNTs grown on: a) 0,5 nm Fe; b) 1,0 nm ; c) 4 nm Fe thin films.

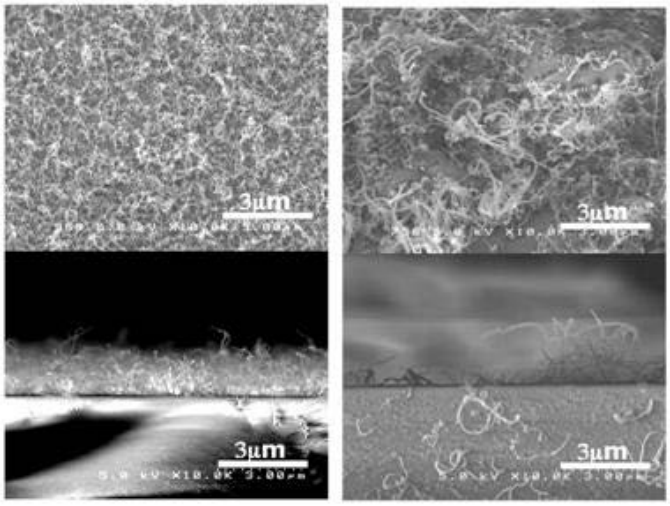

Fig. 9. SEM observations of CNTs grown on: a) thin wet coated 0.01% 40 µl (liquid) $FeCl_2$ and b) $FeCl_2$ powders (control experiment)

This unique method does not require the thin film deposition step, which shortens the time used for each batch of CNT growth [30]. The simplicity of this method allows an easy scale-up for mass production of CNTs with a low cost.

CONCLUSION

In this work we have explored the condition for growing CNTs from petroleum cokes.

We have concluded that, the addition of H_2 in the He carrier gas is a key factor to grow high quantity and more strength CNTs.

Possible mechanism is to enhance the dissociation of higher order of hydrocarbon, remove carbon atoms weakly bonded on the surface of CNTs, and prevent the deactivation of the catalyst.

The control of the amount of hydrocarbon molecules from cokes is also a key factor. It is also important not to

supply hydrocarbon molecules before the catalyst is activated.

Wet-coated thin films of $FeCl_2$ works well as catalyst in the CNT growth process. This process is simplicity and suitable for mass production of CNTs.

Acknowledgements

Authors would like to thanks Prof. Yoshikazu Nakayama from Osaka University for discussion of the results.

[1] *S. Iijima, , Nature (London, United Kingdom)*, 354, (1991), p. 56

[2] Peter J.Harris. Carbon nanotubes ad related structures. Book, Cambridge Univertsity, 1999, p.277

[3] *M.S. Dresselhaus, G. Dresselhaus, and, R. Saito, Physical Review B*, 45, (1992), p. 6234.

[4] *J.W. Mintmire, B.I. Dunlap, and C.T. White. Physical Review Letters*, 68, (1992), p. 631.

[5] *N. Hamada, S. Sawada, and A. Oshiyama. Physical Review Letters*, 68, (1992), p. 1579.

[6] *S. Iijima and T. Ichihashi. Nature* 363, 1993, p.603

[7] *T.W. Ebbesen and P.M. Ajayan, Nature* 358, 1992, p.220

[8] *J.C. Charlier and S. Iijima, Topics in Applied Physics* 80, 2001, p.55.

[9] *J.A. Gómez, A. Marquez, A. Pérez, and A. Duarte-Moller. Advances in Materials Science and Engineering*, v. (2012), Article ID 258673, 7 p.

[10] *B. Krause, M. Ritschel, Ch. Tɔschner, S. Oswald, W. Gruner, A. Leonhardt, P. Petschke. Composites Science and Technology* 70 (2010) 151–160

[11] *M. Mayne, N. Grobert, M. Terrones, R. Kamalakaran, M. Ruhle, H. Kroto, D. Walton. Chemical Physics Letters* 303 _1999. 467–474

[12] *Barreiro, C. Kramberger, M.H. RuËmmeli, A. GruËneis, D. Grimma,,S. Hampel, T. Gemming, B. Buechner, A. Bachtold, T. Pichler. Carbon* 45 (2007) 55–61

[13] *R. Andrews a, D. Jacques a, A.M. Rao, F. Derbyshire, D. Qian, X. Fan, E.C. Dickey , J. Chen e Chemical Physics Letters* 303 _1999. 467–474

[14] *G. Albert, Nasibulin, Anna Moisala, Hua Jiang and Esko I. Kauppinen.* Journal of Nanoparticle Research (2006) 8: 465–475

[15] *M.S. Bell, K.B.K. Teo, and W.I. Milne,* J. Phys. D: Appl. Phys. 40, 2285_2007_.

[16] *J.B.O. Caughman, L.R. Baylor, M.A. Guillorn, V.I. Merkulov, D.H. Lowndes, and L.F. Allard,* Appl. Phys. Lett. 83, 1207 ,2003

[17] *T.Y. Lee, J.H. Han, S.H. Choi, J.B. Yoo, C.Y. Park, T. Jung, S. Yu, W.K. Yi, I. T. Han, and J. M. Kim,* Diamond Relat. Mater. 12, 851 ,2003

[18] *P.E. Nolan, D.C. Lynch, and A.H. Cutler,* J. Phys. Chem. B 102, 4165,1998.

[19] *M. Chhowalla, K. B. K. Teo, C. Ducati, N. L. Rupesinghe, G. A. J.Amaratunga, A. C. Ferrari, D. Roy, J. Robertson, and W. I. Milne,* J. Appl.Phys. 90, 5308 ,2001.

[20] *Y.S. Woo, D.Y. Jeon, I.T. Han, N.S. Lee, J.E. Jung, and J.M. Kim,* Diamond Relat. Mater. 11, 59 ,2002

[21] *S.H. Lim, H.S. Yoon, J.H. Moon, K.C. Park, and J. Jang,* Appl. Phys.Lett. 88, 033114 ,2006

[22] *L. Delzeit, I. McAninch, B. A. Cruden, D. Hash, B. Chen, J. Han, and M.Meyyappan, J. Appl. Phys*. 91, 6027 , 2002.

[23] *Ch. Muller,A.Leonhardt, M. Kutz, and B. Büchner, H. Reuther ,* J. Phys. Chem. *C* 2009, *113,* 2736–2740

[24] *T. Nagasaka, T. Sakai, K. Hirahara, and Y. Nakayama:* Proc. Korea-Japan Joint Symp., Kyoto, 2007, p.36.

[25] *A.G. Nasibulin, David P. Brown, P. Queipo, D. Gonzalez, H. Jiang, A.S. Anisimov, and E. I. Kauppinen.* Phys. stat. sol. (b) 243, No. 13, 3087–3090 (2006)

[26] *N. Nagaraju, A. Fonseca, Konya, and J.B. Nagy,* (2002). Journal of Molecular Catalysis A: Chemical, 181: 57.

[27] *J.W. Seo, K. Hernadi, Miko, and L. Forro,* (2004). Applied Catalysis A: General, 260: 87.

[28] *Y. Li, W. Kim, Y. Zhang, M. Rolandi, D. Wang, and H. Dai,* J. Phys. Chem. *B* 105, 11424 (2001).

[29] *S. Huang, M. Woodson, R. Smalley, and J. Liu,* Nano Lett. 4, 1025 (2004).

[30] *Thomas Laude, Hiroaki Kuwahara, Kazuhiko Sato.* Chemical Physics Letters 434 (2007) 78–81.

Received: 17.09.2013

FORMATION OF NANODIMENTIONAL LAYERS OF TERNARY SOLID SOLUTIONS ON GaSb PLATES SURFACES BY SOLID-PHASE SUBSTITUTION REACTIONS

V.I. VASIL'EV[1], G.S. GAGIS[1], N.N. MURSAKULOV[2], N.N. ABDULZADE[2], A. PARIMBEKOV[3]

[1] Ioffe Physico-Technical Institute of the Russian Academy of Sciences
26 Polytekhnicheskaya st., St Petersburg 194021, Russian Federation
Fax: (812) 297 1017 Phone: (812) 292 7914 e-mail: giman@mail.ioffe.ru
[2] Institute of Physics of Azerbaijan National Academy of Sciences,
33, H.Cavid ave., Az-1143, Baku, Azerbaijan
e-mail: nmursakulov@physics.ab.az
[3] Semey State University named after Shakarim,
20 "A" Glinki, Semey, Kazahstan

The results of investigations of processes of formation of ternary solid solutions of GaPSb and GaAsSb on monocrystal GaSb plates are presented. We propose a new technology of obtaining nanodimensional layers of GaPSb and GaAsSb ternary solid solutions on the surface of GaSb semiconductor crystals by replacing their Sb atoms with P or As atoms delivered from the gas phase. The sources of phosphorous or arsenic gases was GaP-Sn, GaP-Ga, $ZnSnP_2$-Sn, $ZnSnAs_2$-Sn solutions. The solutions and GaSb (100) plates were charged in a closed graphite cassette and the process was carried out at 500–600°C in a quartz reactor filled with hydrogen. Phosphorus or arsenic is supplied to the surface of GaSb semiconductor crystals in the form of dimers or tetramers molecules. In the course of nanodimensional layer formation on the heated surface of a semiconductor crystal, dimers and tetramers exhibit reversible decomposition into atoms, which diffuse into the surface layer of GaSb and replace antimony atoms because the Ga–P or Ga-As binding energy is greater than that of Ga–Sb bonds. The composition and thickness of formed solid solution nanolayer depend on technology parameters, such as time of process, temperature and pressure of arsenic or phosphorous vapors. When $ZnSnP_2$ or $ZnSnAs_2$ solution in Sn and n-GaSb are using, the p-n-junction together with solid solution nanolayer is formed. The ternary solid solution on GaSb surface improves photoluminescent characteristics several times more than GaSb.

KEY WORDS: arsenic or phosphorous vapors, nanodimensional layers of GaPSb and GaAsSb, closed graphite cassette,
PACS: 42.70.Km; 68.35.Dv; 68.60.Dv; 73.61.Ga; 78.66.Hf; 81.15.Cd

At present, semiconductor structures with nanodimensional regions are fabricated predominantly by the method of molecular beam epitaxy (MBE) and metalorganic vapor phase epitaxy technique [1]. Both these technologies are rather expensive. Therefore, it is an important task to develop cheaper methods - in particular, for large scale production of GaAs based photovoltaic converters (PVCs). To date, a rather high level of the conversion efficiency (up to 20–25%) has been achieved for PVCs based on GaAs plates with p–n junctions formed by zinc diffusion from the gas phase [2]. Using of tandem PVCs consisting upper cascade based on GaAs and lower cascade based on GaSb allows to increase conversion efficiency about 6% more [3]. The role of lower cascade GaSb is the absorption and conversion of the mid infrared spectral range radiation.

An additional increasing the efficiency of PVCs can be achieved by forming the so-called wide-band gap optical window (WOW) layer transparent for radiation to be converted, which is isomorphous with the base material and matched to it without defects. The WOW to a considerable degree suppresses the nonradiative recombination processes related to surface states. A rather cheap method of WOW formation is based on liquid phase epitaxy (LPE), which can provide for the formation of a wide-bandgap GaAlAs layer on the GaAs crystal surface [4]. But several method for forming WOW on GaSb cascade is not widely used.

In this latter we propose a new technology of obtaining nanodimensional layers of GaPSb or GaAsSb ternary solid solutions on the surface of GaSb semiconductor crystals by replacing their Sb atoms with P or As atoms delivered from the gas phase. The bandgap value of solid solutions GaPSb or GaAsSb increases with increasing of P or As containing, that means this materials are suitable for WOW formation on GaSb, because they have greater bandgap value.

Used method of obtaining of thin films of GaAsSb and GaPSb on GaSb is similar to one described by us in [5].

In the present study, phosphorus vapor was produced by evaporating of GaP-Sn, GaP-Ga, $ZnSnP_2$-Sn, $ZnSnAs_2$-Sn solutions. The solutions and GaSb (100) plates were charged in a closed graphite cassette and the process was carried out at 500–600°C in a quartz reactor filled with hydrogen. Phosphorus or arsenic is supplied to the surface of GaSb semiconductor crystals in the form of dimers or tetramers molecules. In the course of nanodimensional layer formation on the heated surface of a semiconductor crystal, dimers and tetramers exhibit reversible decomposition into atoms, which diffuse into the surface layer of GaSb and replace antimony atoms because the Ga–P or Ga-As binding energy is greater than that of Ga–Sb bonds.The properties of formed by describing methods solid solutions depend on delivered on GaSb atoms As or P quantity and depth of their permeation.

The quantity of delivered on surface of GaSb atoms depends on vapor of As or P pressure and on exposure time. It can be observed by investigation of GaSb plates in phosphorous vapor processing.

It Is known that the photoluminescence (PL) spectra of undoped GaSb usually contain two bands. The first one (fig. 1, peak 1) is associated with transitions on stoichiometric defect level (vacancies of Sb, atoms of Ga on the Sb places), which behaves similar impurities. The second one is associated with unterband transitions (fig. 1, peak 2).

PL of undoped GaSb mainly associated with transitions on stoichiometric defect level, interband transitios are not observed (fig 1, curve GaSb).

When saturated solution Ga-GaP at 540 - 580 °C is using as vapor of phosphorous source to processing undoped GaSb plate, the solubility of phosphorous in Ga is size of order 10^{-4} [6], the vapor pressure of P_2 molecules over such solution makes up the value size of order 0.01 Pa. In this case the concentration of phosphorous delivered on plate surface is little, but sufficient to elimination of defects that are nonradiative recombination centers. In that way the curriers fill up the free states not only on stoichiometric defect level, but and in conduction band, and the both peaks: the peak of stoichiometric defect transitions and peak of interband transitions are observed (fig 1, curve GaSb:P).

When the plate of GaSb:Te be exposed to processing in vapor of phosphorous with two orders more pressure (vapor source is 5% solution of $ZnSnP_2$-Sn at 585 °C), at kindly exposure times (10 – 20 min) the PL intensity increasing relatively one of unprocessed GaSb:Te plate can be observed. We observe increasing of PL intensity about 3-5 times more at 77 K, that can means that the GaPSb solid solution layer plays the role of WOW. The WOW effect indicates that the phosphorous atoms stand in places in the crystal lattice sites, so solid-phase substitution reactions take place.

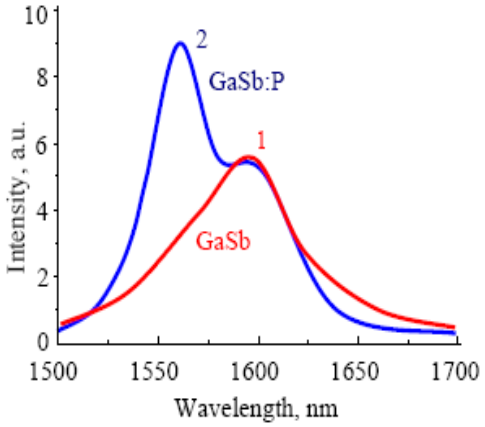

Fig. 1. The PL at 77 K spectra of GaSb (curve GaSb) and GaSb exposed in phosphorous vapor with pressure size of order 0.01 Pa (curve GaSb:P). 1 – peak of stoichiometric defect level transitions, 2 – peak of interband transitions.

When the quantity of phosphorous atoms delivered on surface of GaSb is too large, that can take place at high exposure times (30 min and more) or at higher vapor pressures, the intensity of PL decreases. The higher the concentration of phosphorus in GaPSb solid solution, the greater the lattice misfit between GaPSb and GaSb crystalline structures. At small thicknesses, the GaPSb layer can be elastically deformed and thus conjugated with the GaSb lattice with a relatively small number of structural defects.

At the concentration of phosphorous about 20 % in surface layer of plate and depth of permeation about 1000 nm (fig. 2), the PL intensity sufficiently decreases relatively one of unprocessed GaSb:Te plates. At higher times of exposure at the same temperature and vapor of phosphorous pressure, the PL of obtained samples is not observed.

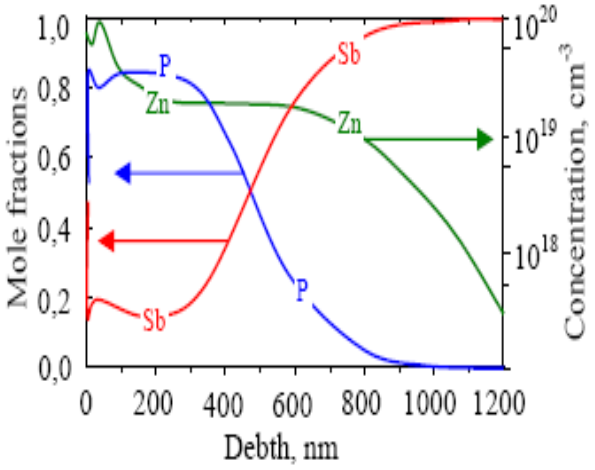

Fig. 2. The distribution of components P, As and Zn on GaSb sample with formed solid solution nanolayer (vapor of phosphorous source is 5% solution of $ZnSnP_2$-Sn at 585 °C, exposure time 30 min).

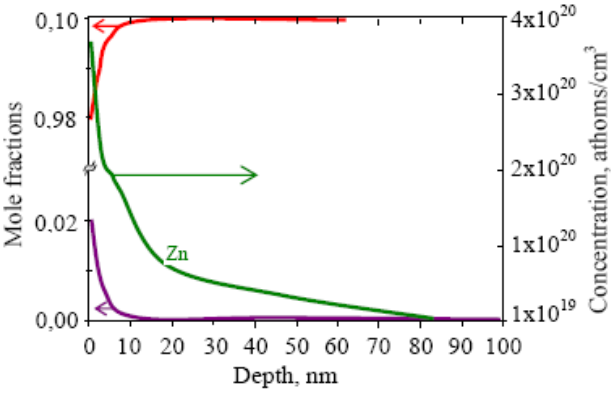

Fig 3. The distribution of components As, Sb and Zn on GaSb sample with formed solid solution nanolayer (vapor of arsenic source is 5% solution of $ZnSnAs_2$-Sn at 580 °C, exposure time 15 min).

So, the composition and thickness of formed solid solution nanoleyer depend on technology parameters, such as time of process, temperature and pressure of arsenic or phosphorous vapors. We determinate that optimal exposure times for forming GaAsSb or GaPSb WOW on GaSb surfaces at 580 – 600 °C using vapor sources $ZnSnP_2$-Sn or $ZnSnAs_2$-Sn solutions containing about 5% P or As is amounted 10 – 20 min. At this condition the distribution of permeating component has exponential shape (fig. 3).

When $ZnSnP_2$ or $ZnSnAs_2$ solution in Sn and n-GaSb are using, the p-n-junction together with solid solution nanolayer is formed. The p-n-junction lay below the GaPSb or GaAsSb WOW because the depth of Zn diffusion is larger than one for As or P (fig 2, 3).

So, proposed method can be used as cheap technology of forming GaSb cascade with WOW for tandem PVC.

ACKNOWLEDGEMENTS: This work has been supported by STCU - Grant № 5611

[1]. *A.B. Krysa, J.S. Roberts, D.G. Revin, K. Kennedy, L.R. Wilson, and J.W. Cocburn,* Proceedings of Symp. "Semiconductor Lasers: Physics and Technology" (November 5–7, St. Petersburg, 2008), p. 15 [in Russian].

[2]. *V.M. Andreev, V.P. Khvostikov, V.R. Larionov, V.D. Rumyantsev, E.V. Paleeva, and M.Z. Shvarts.* High-efficiency AlGaAs/GaAs concentrator (2500 suns) solar cells. Semiconductors, 33, 976 (1999).

[3]. *V.M. Andreev, S.V. Sorokina, N.Kh. Timoshina, V.P. Khvostikov, M.Z. Shvarts.* Solar cells based on gallium antimonide. Semiconductors May 2009, Volume 43, Issue 5, pp 668-671.

[4]. *V.I. Vasil'ev, I.P.Nikitina, V.M. Smirnov, and D.N. Tretyakov.* Isoperiodical heterostructures GaInAsSb/GaSb grown by LPE from Sb-rich melts in spinodal decomposition area. Mater. Sci. Eng. 66, 67 (1999).

[5]. *V.I. Vasil'ev, G.S. Gagis, V.I. Kuchinskii, V.P. Khvostikov, E.P. Marukhina.* Obtaining Nanodimensional Layers of GaAsP Solid Solutions on GaAs by Solid_State Substitution Reactions, Technical Physics Letters, 2013, Vol. 39, No. 5, pp. 472–474

[6]. Solubility of III-V Compound Semiconductors in Column III Liquids. R.N.Hall. Journal of The Electrochemical Society, May 1963, Vol 11.

Received: 09.09.2013

INFLUENCE OF ELECTRIC FIELD ON THERMOPHYSICAL AND STRENGTH PROPETIES OF COMPOSITIONS ON THE BASE OF POLYVINYLINIDE FLUORIDE AND PIESOCERAMICS

H.S. IBRAGIMOVA
Institute of Physics of Academy of Sciences of Azerbaijan
AZ-1143, Baku , H. Javid ave., 33

The results of electric field influence on thermophysical and strength properties of composition materials on the base of polyvinylinide fluoride (PVDF) and piesoceramics of PCP5 and PCP8 types are given in the given work. The correlation between changes of strength and thermophysical properties of the investigated compositions is established.

Keywords: polyvinylinide fluoride (PVDF), piesoceramics of PCP5 type, piesoceramics of PCP8 type.
PACS: 543.621

The polymer materials at the use in the capacity of different products in the dependence on assignment are treated by different external influences, such as electric discharges, heat, ionizing radiation and etc. Moreover, the changes of different physicochemical and electrophysical strength properties take place [1]. It is revealed that different effects mainly electrotreatment can influence not only on dielectric and electrophysical properties of polymer composites but on other ones including thermophysical properties. The change character of polymer composite thermophysical properties at both high and low temperatures gives the information about their internal structure [2]. The aging processes of polymer composites involve the more deep layers and as a result of which changes take place in some of them, i.e. these effects influence on thermophysical properties.

In the present work the investigation results of electric field influence on mechanical and electric strengths, on composite thermophysical properties on the base of polyvinylinide fluoride containing the piesoceramic materials PCP5 and PCP8 having the rhombohedral and tetragonal structure correspondingly are given. PCP5 and PCP8 ceramics have the zirconate-titanate-lead composition. The particle sizes of piesoceramics are d≤ 5μm. [3]

The compositions are obtained by hot pressing method at melting point of polymer matrixes under pressure 15MPa during 10 min with following cooling up to room temperature with velocity 2000degr/min. The polymer compositions are treated during 1 hour under influence of electric field below punch-through voltage in alternating electric field at different strengths.

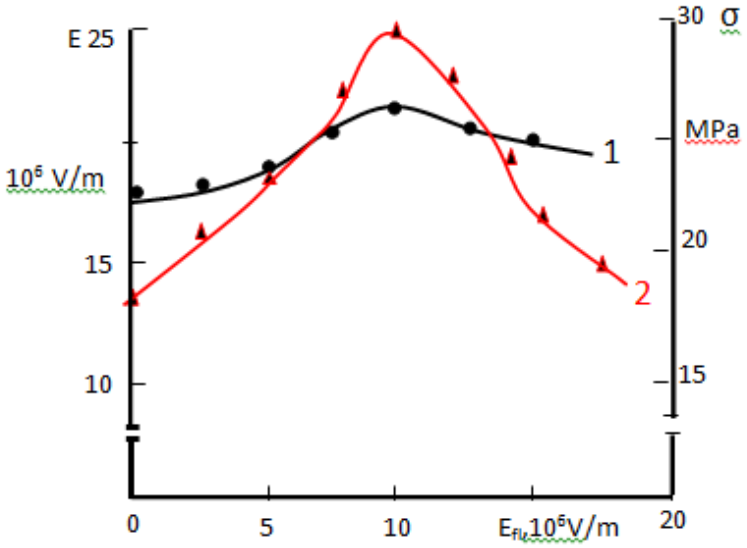

Fig.1. The dependence of electric (1) and mechanical (2) strengths of PVDF +30%vol. PCP5 composition on electrotreatment field strength during 1 hour.

The dependence of electric and mechanical strengths of PVDF + PCP5 composition in component relation 70+30% on electrotreatment field strength during 1 hour is given on fig.1. It is seen that electrical and mechanical strengths achieve their maximal values at electric field strength $E_{tr.}=10^7$V/m. By our opinion it is connected with overheating of polymer matrix and as a result with joining of polymer molecular chains.

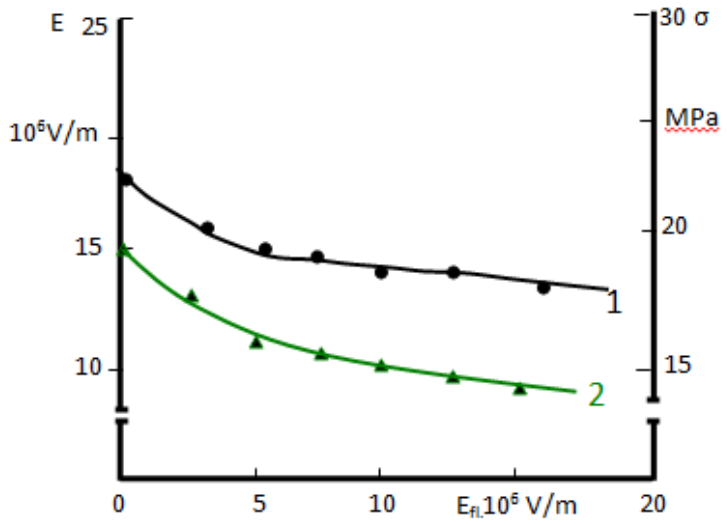

Fig.2. The dependences of electrical (1) and mechanical (2) strengths of composition PVDF +30%vol.PCP8on electrotreatment field strength.

The composite material PVDF+30%vol.PCP5 becomes more heat stable ones with increase of electric field strength and thermodestruction activation energy increases in comparison with E=0 (tab.). The last one evidences about the fact that composite crystallinity degree increases with increase of electric field influence, that's why the more high energy is required on bond destruction. For the composite material PVDF +30%vol.PCP8 (fig.2) the thermodestruction beginning shifts to the side of high temperatures with increase of electric field strength. It is also defined that these composition characteristics on the base of PCP5 piesoceramics are bigger ones than PCP8 one. It can be explained by structures of PCP5 and PCP8 piesoceramics. It is known that piesoceramics PCP5 has the big value of reorientation polarization and electronegativity increasing the adhesion of polymer matrix and piesoceramics than PCP8 piesoceramics. Also PCP5 piesoceramics has the rhombohedral structure and PCP8 piesoceramics has tetragonal structure. The calculation results of activation energy of thermodestruction of PVDF+30%vol.PCP5and PVDF +30%vol.PCP8 compositions are given in table.

Table

Composite composition	Electric field strength $E \cdot 10^6$V/m	Thermodestruction temperature in°C		Activation energy of thermodestruction E_{act} in joule/mol	Mechanical strength (MPa)	Electric strength ($E \cdot 10^6$V/m)
		beginning	final			
PVDF + PCP5 (70/30)	0 5 10 15	95 98 110 105	405 410 420 415	163,45 173 190,89 180	18 25 30 27	18 20 22 20
PVDF +PCP8 (70/30)	0 5 10 15	110 100 85 70	360 300 260 200	192,9 190,09 137,17 110	17 14 12 11	15 11 9 5

Note that if mechanical and electrical strengths in dependence on electrotreatment field strength increases up to $E_{tr.}=10 \cdot 10^6$ V/m and further decreases in the case of PVDF+30%vol.PCP5 composition, then in the case of PVDF+30%vol.PCP8composition the strengths only decrease in the dependence on $E_{tr.}$

Thus the established correlation between changes of strength and thermophysical properties of PVDF +30% PCP5 compositions is explained by the fact that the bigger composition strength the higher thermal stability and bigger thermodestruction activation energy of this composition in dependence on $E_{tr.}$ For PVDF +30%vol.PCP8 the heat stability and activation energy decrease at decrease of mechanical and electric strengths. By our opinion it is connected with filler structure, i.e. because of the structure the composition crystallinity degree of PVDF +30%vol.PCP5 is bigger than PVDF +30%vol.PCP8 composition and under influence of electric fields the destruction process behavior time increases

[1] *S.A. Abbasov, M.A. Ramazanov, Kh.S. Ibragimova, Z.E. Mustafayev.* Fizika i khimiya obrabotki materialov, 2003, n.5. s.26-29. (in Russian)

[2] *V.S. Gorshkov, V.V. Timashev, V.G. Savelyev.* Metodi fiziko-khimicheskogo analiza vyajushikh veshestv. M. Visshaya shkola, 1981, s.37-42. (in Russian)

[3] *M.A. Bagirov, V.P. Malin, S.A. Abasov*. Vozdeystvie elektricheskikh razryadov na polimernie dielektriki. Baku, Elm, 1975, s.168. (in Russian)

[4] *S.A. Abbasov, Kh.S. Ibragimova, M.A. Ramazanov.* Fizika, 2007, v.13, n.1-2 s.137-138. (in Russian)

Received: 24.09.2013

ELECTRON STRUCTURE AND DYNAMIC PROPERTIES OF ALLATOSTATIN MOLECULES

L.I. VELIYEVA, E.Z. ALIYEV
Baku State University, AZ1148, Z. Khalilov street, 23, Baku, Azerbaijan
Lala Veliyeva@rambler.ru

The electron structure and dynamic properties of allatostatin molecules are investigated, the stable elements of space structure are revealed, the quantitative estimation of dihedral angle limit changes of the peptide molecule main chain is carried out in the process of dynamic reconstructions by MM+ and MNDO methods.

Keywords: allatostatins, space structure, electronic structure, dynamic properties.
PACS: 87.80.-y

INTRODUCTION

The study of electronic structure and conformational-dynamic properties of biological molecules including the neuropeptides becomes more actual one in the connection with high degree of development of computer technology and more distribution of corresponding program products. The investigations in this direction are also actual ones from the point of view of one important problem solution of the modern science and their functional activity. The neuropeptides of allatostatin family having the unique ability to regulate the synthesis processes and emission of juvenile hormones of insect different types are related to object number of intensive investigation of last decade. [1-4]. The allatostatin family includes the peptide molecules known as allatostatins I-IV or Dippu-ASTs.

In the given work the dynamic properties of allatostatins are investigated by molecular mechanics MM+, the stable elements of space structure are revealed, the quantitative estimation of dihedral angle limit changes of the peptide molecule main chain in the dynamic reconstruction process is carried out. The electron structure of allatostatins is investigated by semiemperical method of quantum chemistry MNDO in standard parameterization and comparative analysis of obtained results is carried out.

CALCULATION METHODS

The methods of quantum chemistry and molecular dynamics have the wide distribution in numerical modeling of electronic and atomic structures of complex molecular systems. Nowadays the enough modern computing complexes realizing the calculations by the methods of quantum chemistry and molecular dynamics are known. The complex of quantum-chemical and molecular-dynamic programs **HyperChem** is related to the number of such functioning program products. All results of electron and molecular-dynamic modeling presented in the given work are obtained with the use of this program, the demonstrative version of which is accessible on site http://www.hyper.com [5-7]. The calculative molecule models are constructed on the base of atom coordinates obtained by the method of theoretical conformational analysis within the framework of atom mechanical model [8-11]. The neuropeptide optimal electronic structure is established in optimization process of valence electron energy at fixed coordinates of atom nuclei. The molecule general charge in the ground state is taken equal to zero at calculations of electronic structure. The values of total, atomic and electron energies, dipole moments are calculated and the charge distribution on atoms of the molecules under consideration is investigated. The change character of atom partial charges in the dependence on conformational states of the investigated molecules is studies. The neuropeptide N-end is modified by acetyl (ACE) and C-end is modified by N-metilamin (NME) with formation of two additional peptide bonds with the aim of decrease of edge effect influence from strongly polar end groups.

CALCULATION RESULTS AND THEIR DISCUSSION

The low-energy conformational states of allatostatins before and after molecular dynamics carried out during 30psec at constant temperature 273K are given on fig1- 4. The neuropeptide molecule relaxation with use of force field MM+ is carried out before calculation. The electronic parameters of investigated molecules calculated by MNDO method are generalized in table 1.

Allatostatin I. Allatostatin I-neuropeptide in chemical structure of which are thirteen aminoacid residuals: Ala1-Pro2-Ser3-Gly4-Ala5-Gln6-Arg7-Leu8-Tyr9-Gly10-Phe11-Gly12-Leu13. The conformation corresponding to global minimum of conformational energy according to conformational analysis data and conformation obtained to the end of dynamic transformations in processes of molecular dynamics are given on fig.1a.

The analysis of obtained results shows that molecule energy changes during first five picoseconds take place, further, in simulation process the fluctuation character becomes monotonous one. The energy achieves its minimal value to the end of time interval (5-30psec) that evidences about stabilization of space structure. As it is followed from calculation results, the section of peptide chain Leu8-Leu13 forming β-rotation is more stable one in comparison with section Ala1-Gln6 on N-end of peptide molecule. This result agrees with conformational analysis data according to which β-rotation on section Leu8-Leu13 realizes in 70% of calculated low-energy states of allatostatin I molecule.

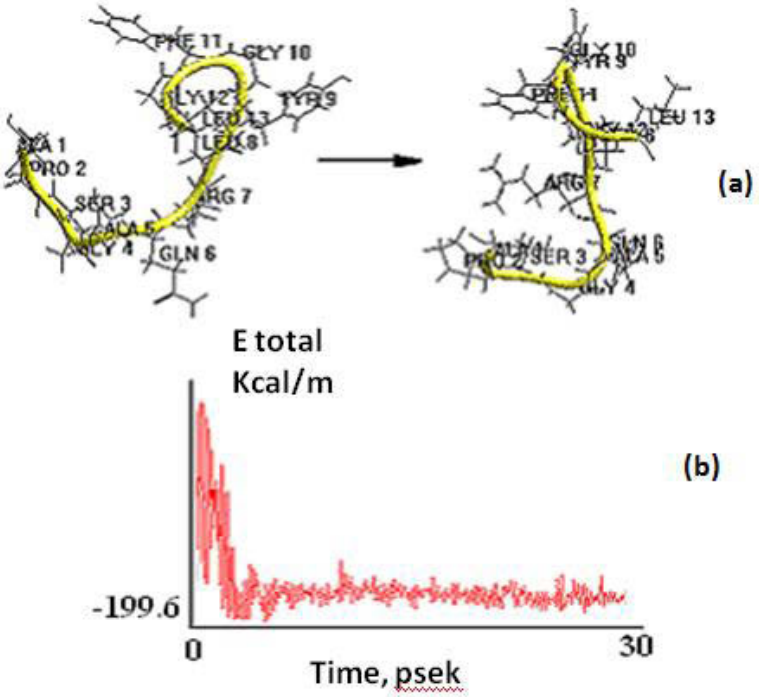

Fig.1. Conformational transformations (a), change of total energy (b) of allatostatin I in process of molecular dynamics.

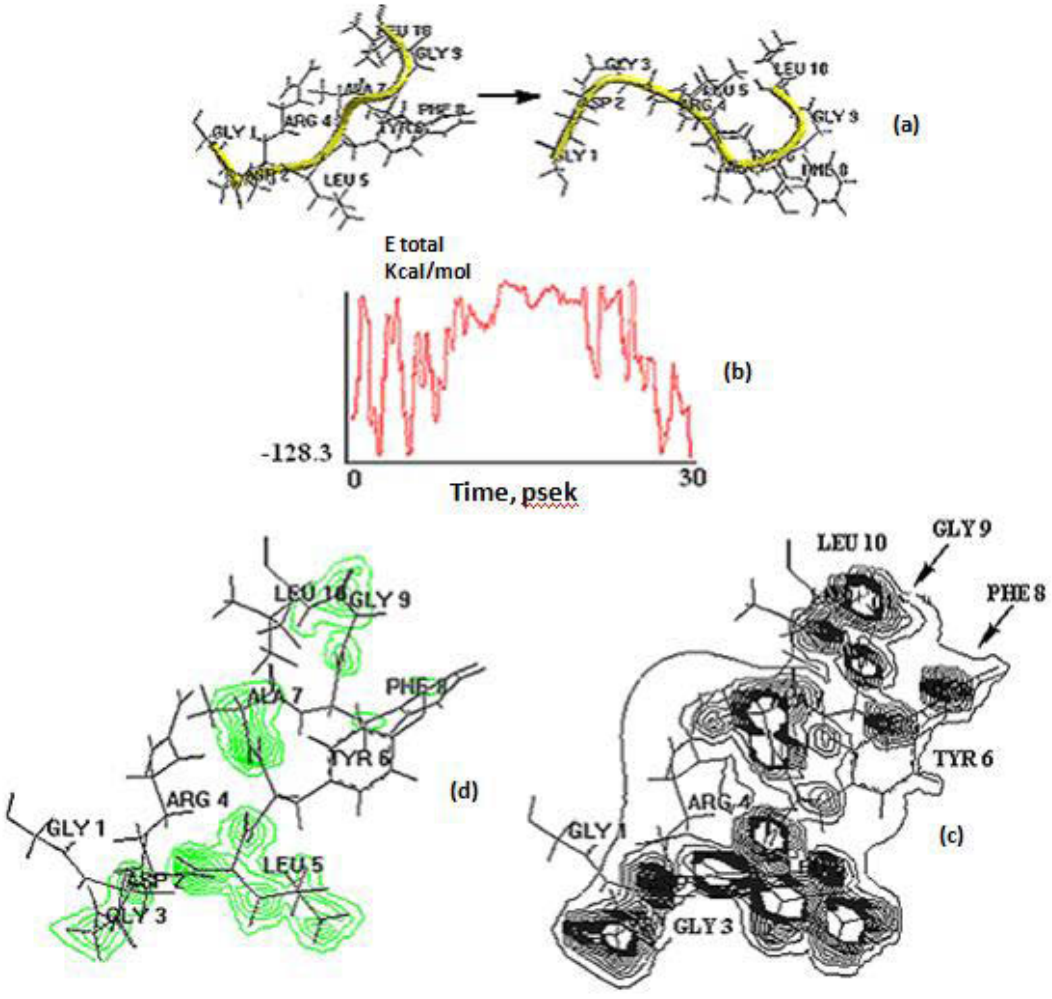

Fig.2. The conformational transformations (a), total energy change (b), electrostatic potential distribution (c) and charge density distribution (d) on XY plane obtained for allatostatin II.

Allatostatin II. Allatostatin II-neuropeptide consists of consistency of aminoacid residual decade: Gly1-Asp2-Gly3-Arg4-Leu5-Tyr6-Ala7-Phe8-Gly9-Leu10. The conformation corresponding to global minimum of conformational energy according to conformational analysis data, is given on fig.2a [8].

The molecule consists the arginine residual (Arg4) with positively charged side radical and residuals with aromatic side chains (Tyr6, Phe8). The negatively charged carboxylated group of side chain of asparaginic acid residual (Asp2) and volume side chain in leucine residual (Leu10) are also related to number of functional important groups defining the space structure peculiarities of molecule. According to results of conformational analysis the presence of labile C-end section at relatively hard N-end fragment is the space structure peculiarity of molecule. As it is followed from calculation results, the molecule energy change has the non-monotonous character, the energy fluctuations on whole expansion of dynamic process are observed. The energy strong decrease which achieves the minimal value-128.3 kcal/mol is observed to simulation end. In space structure of allatostatin II the formation of two β-rotations in tops of which are residuals Arg4 and Phe8, is observed. After molecule relaxation the quantum-chemical calculations by MNDO method are carried out. Any quantum-chemical calculation is based on minimization of system energy of N electrons and M nuclei. The minimum search methods allow us to find the point on potential energy surface responding to molecule equilibrium configuration with least energy (or minima if they are several ones). The choice of the initial geometry and molecule symmetry play here the important role: correctly taking into consideration the symmetry because of the decrease of varied parameters the calculation time can be decreased in several times. The conjugated gradient method is used in calculations. The quantum-chemical method is also used for calculations of dipole moment and construction of distribution picture of molecular electrostatic potential and charge density for allatostatin molecules. The molecular electrostatic potential is defined by electron density ρ(r) and nuclear charges Z. The potential characterizes the electrostatic interaction energy between molecular (positive and negative) charge distribution and positive unit infinitesimal charge.

Allatostatine III. The initial structure of Allatostatin III-neuropeptide contains the consistence of nine amino-acid residuals Gly1-Gly2-Ser3-Leu4-Tyr5-Ser6-Phe7-Gly8-Leu9. The starting structure for molecular-dynamic calculations corresponds to the state of minimal value of conformational e n ergy obtained as a result of molecule conformational analysis of allatostatin III molecule [9]. As it is followed from calculation results, the strong molecule energy change in simulation process takes place during first five psec. The increase of distance between end groups of Gly1 and Leu9 residuals (increase takes place in limits 6.1÷7.3 Å) is the result of such increase, which however doesn't destroy the character elements of allatostatin III molecule space structure, in particular, folded structure on section Leu4-Phe7 is saved on all extension of molecular dynamics.

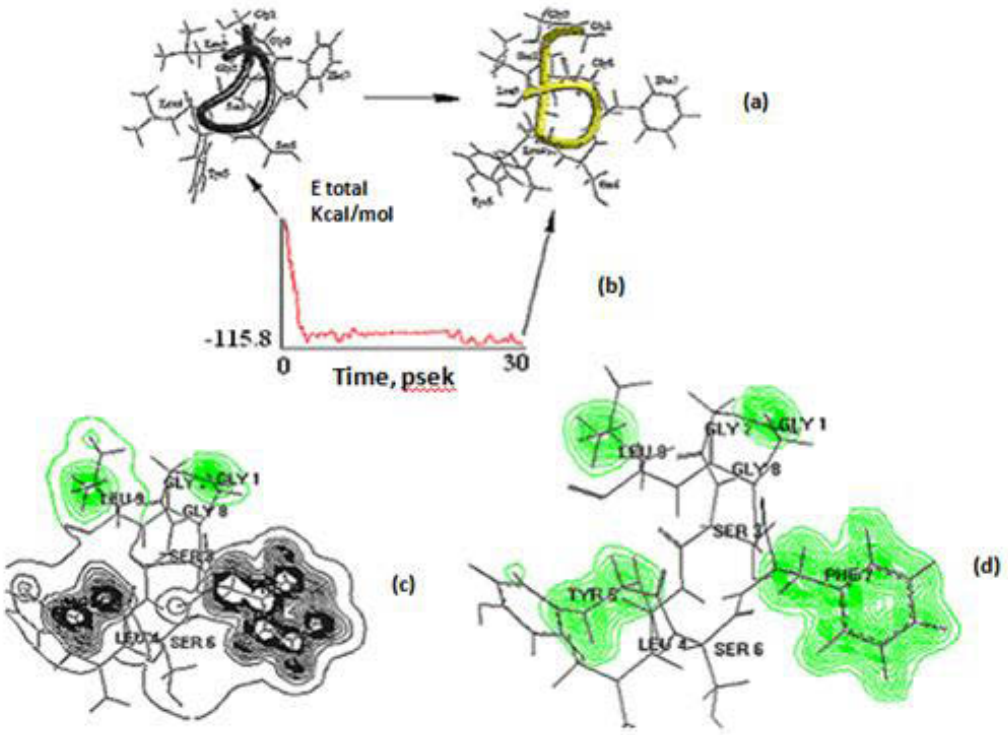

Fig.3. Molecular dynamic of allatostatin III (a), the molecule total energy change (b), electrostatic potential distribution (c) and charge density distribution (d) on XY plane

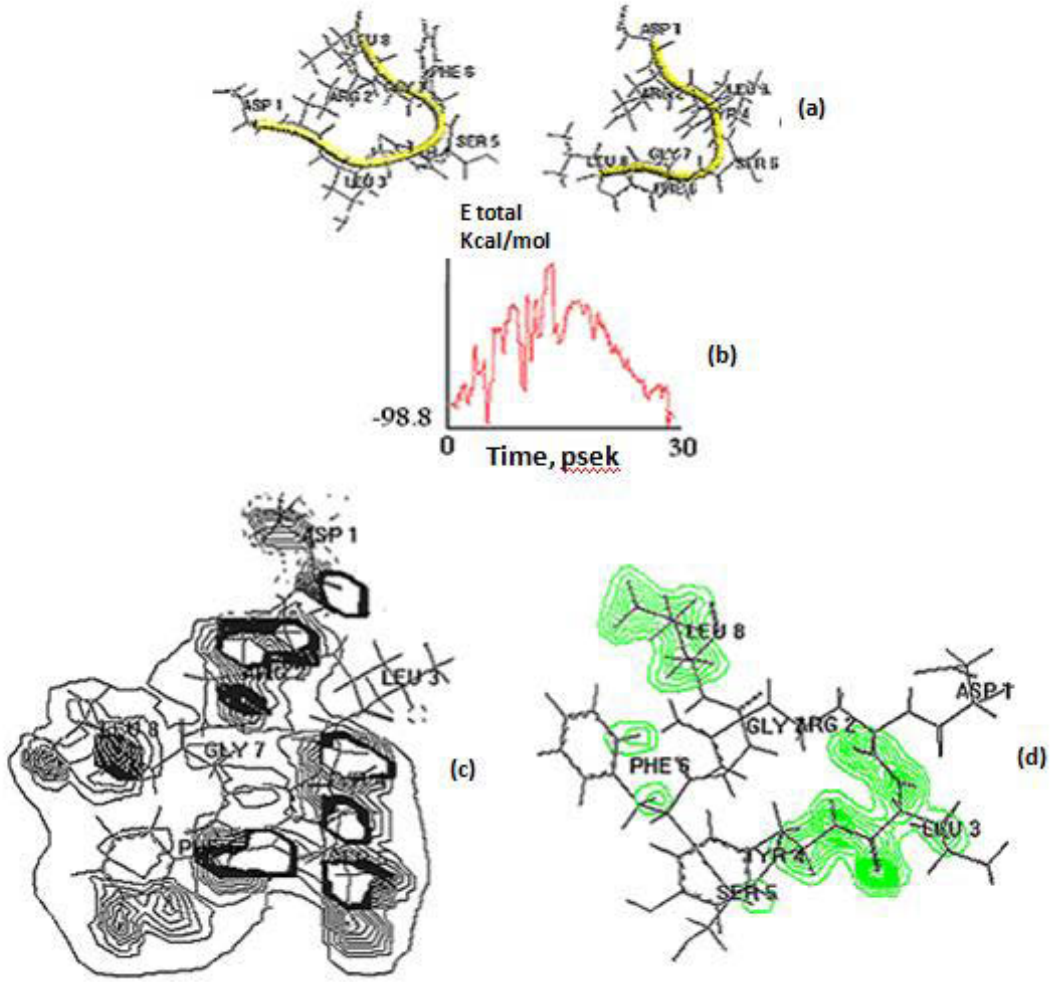

Fig.4. Molecular dynamics of allatostatin (a), the molecule total energy change (b), electrostatic potential distribution (c) and charge density distribution (d) on XY plane

Allatostatine IV. The eight consequently fixed amino-acid residuals Asp1-Arg2-Leu3-Tyr4-Ser5-Phe6-Gly7-Leu8 are in primary structure of allatostatin **IV**. The conformational, corresponding to global minimum of conformational energy according to conformational analysis data, is given on fig.4,a [10,11].

The significant conformational mobility of N-end consequence in comparison with tetra-peptide fragment Tyr4-Leu8 is established in process of molecular dynamics. The energy change has the non-monotonous character, achieves the maximal value at 12 psec, further the monotonous decrease and further relaxation of molecule structure take place.

The obtained results will be used for molecular modeling of neuropeptide analogues and study of their structure-functional interaction with the aim of general elements of space structure responsible for pharmacological effects of investigated compounds.

[1] *D. Veelaert, B. Devreese, L. Schoofs et al.* «Izolation and characterization of eight myoinhibiting peptides from the desert locust, Schistocerca gregaria: new members of the cockroach allatostatin family». Mol.Cell Endocrinol., 1996, v.122 (2), p.183-190.

[2] *D. Veelaert, B. Devreese, L. Schoofs et al.* «Izolation and characterization of schistostatin-2 (11-18) from the desert locust, Schistocerca gregaria: a truncated analog of schistostatin-2». Regulatory peptides,1996, v.67 (3), p.195-199.

[3] *W.G. Bendena, B.C. Donly, S.S. Tobe.* «Allatostatins: A growing family of neuropeptides with structural and functional diversity». Ann.N.-Y.Academy of Sciences, 1999, v.897, p.311-329.

[4] *J.P. Edwards, N. Audsley, G.C. Marris, R. Weaver.* «The role of allatostatic and allatropic neuropeptides in the regulation of juvenile hormone biosynthesis in Lacanbia oleracea». Peptides, 2001, v.22(2), p.255-261

[5] *E.E. Shnol, A.G. Grivtsov i dr.* «Metod molekulyarnoy dinamiki v fizicheskoy khimii». M.: Nauka, 1996. (in Russian)

[6] *K.V. Shaytan, S.S. Saraykin.* «Metod molekulyarnoy dinamiki»,1999, (in Russian), http://www.moldyn.ru/library/md/default.htm

[7] http://www.hyper.com

[8] *L.I. Veliyeva, M.A. Musayev, I.N. Aliyeva.* «Strukturnoe issledovanie molekuli allatostatina-II». V materialakh Mejdunarodnoy nauchnoy Konferentsii «Molekulyarnie, membrannie i kletochnie osnovi

funktsionirovaniya biosistem», Minsk, Belarus, 2006, s.111-113. (in Russian)

[9] *I.N. Alieva, L.I. Veliyeva, M.A. Musayev, N.M. Gojayev* «Conformationalal feature s of the Dippu-AST 8 neuropeptide from Cockroach Diploptera punctata». Protein and Peptide Letters, 2006, v.13, p.1007-1015.

[10] *M.A. Musayev*, *L.I. Veliyeva*, *I.N. Alieva. N.M. Gojayev.* «Prostranstvennaya struktura neyropeptida allatostatina-4». Vestnik Bakinskogo Universiteta, seriya fiz-mat. Nauk, 2005, n.2, s.167-178. (in Russian)

[11] *L.I. Veliyeva, M.A. Musayev, I.N. Alieva, N.M. Gojayev* «Molekulyarnaya dinamika neyropeptidov semeystva allatostatinov». Vestnik Bakinskogo Universiteta, seriya fiz-mat. Nauk, 2006, №1, c.120-131. (in Russian)

Received: 27.06.2013

DOUBLE-SPIN ASYMMETRIES IN SEMI-INCLUSIVE DIS

S.K. ABDULLAYEV
Baku State University, Az-1148, Z.Halilov str., 23
s_abdullayev@mail.ru.

The general expressions for the effective cross-sections of semi-inclusive reactions $l^{\mp}N \Rightarrow l^{\mp}hX$, $\nu_{\mu}(\bar{\nu}_{\mu})N \Rightarrow \nu_{\mu}(\bar{\nu}_{\mu})hX$, $\nu_{\mu}(\bar{\nu}_{\mu})N \Rightarrow \mu^{-}(\mu^{+})hX$, $\mu^{-}(\mu^{+})N \Rightarrow \nu_{\mu}(\bar{\nu}_{\mu})hX$ are obtained in the framework of quark-parton model.

Keywords: semi-inclusive reactions, quark-parton model, semi-inclusive, spin asymmetry.
PACS: 13.60.-r, 13.88.+e, 14.20.Dh, 14.65.-q

1. INTRODUCTION

High energy experiment with polarized beams and targets has opened a new window for revealing QCD dynamics and hadron structures. Ongoing RHIC-SPIN, HERMES and COMPASS experiments are going to provide us with a variety of data disclosing spin distribution inside the nucleon. The electron Ion Collider (EIC) at BNL is expected to be a more powerful and sensitive tool for the QCD spin physics. In this paper, we study the hadron production in polarized semi-inclusive DIS off nucleon (they are intensive investigated experimentally, [1-5]):

$$l^{-}(\lambda)+N(h_N)\Rightarrow l^{-}+h^{\pm}+X\,, \quad (1)$$
$$l^{+}(\lambda)+N(h_N)\Rightarrow l^{+}+h^{\pm}+X\,, \quad (2)$$
$$\nu_{\mu}+N(h_N)\Rightarrow \nu_{\mu}+h^{\pm}+X\,, \quad (3)$$
$$\bar{\nu}_{\mu}+N(h_N)\Rightarrow \bar{\nu}_{\mu}+h^{\pm}+X\,, \quad (4)$$
$$\nu_{\mu}+N(h_N)\Rightarrow \mu^{-}+h^{\pm}+X\,, \quad (5)$$
$$\bar{\nu}_{\mu}+N(h_N)\Rightarrow \mu^{+}+h^{\pm}+X\,, \quad (6)$$
$$\mu^{-}(\lambda)+N(h_N)\Rightarrow \nu_{\mu}+h^{\pm}+X \quad (7)$$
$$\mu^{+}(\lambda)+N(h_N)\Rightarrow \bar{\nu}_{\mu}+h^{\pm}+X \quad (8)$$

Where λ is the lepton spirality, h_N is the longitudinal polarization of nucleon target.

The cross-section for the production of a hadron h in the current fragmentation region are given by

$$\frac{d\sigma(\lambda;h_N)}{dxdydz}=\sum_{q,h_q} f_{q(h_q)}^{N(h_N)}(x,Q^2)\frac{d\hat{\sigma}}{dy}D_q^h(z,Q^2)\,, \quad (9)$$

where $f_{q(h_q)}^{N(h_N)}(x,Q^2)$ is the distribution functions of polarized quarks in the polarized nucleon, $D_q^h(z,Q^2)$ is the fragmentation functions of the quark into the detected hadron h, $d\hat{\sigma}/dy$ is the elementary cross-section. The usual DIS variables defined as:

$$x=\frac{Q^2}{2P\cdot q}, \qquad y=\frac{q\cdot P}{k\cdot P}, \qquad z=\frac{P_h\cdot P}{P\cdot q}\,,$$

where k, P, P_h and are the four-momenta of the initial lepton, the target nucleon, the production hadron, and the virtual bozon respectively.

1. Neutral current lepton processes $l^{\mp}N\Rightarrow l^{\mp}hX$

Let us consider first the processes $l^{\mp}N\Rightarrow l^{\mp}hX$; for them there exist two possible elementary contributions:

$$l^{-}+q\Rightarrow l^{-}+q\,, \quad l^{-}+\bar{q}\Rightarrow l^{-}+\bar{q}\,.$$

Taking under the considerations the exchange of x and Z^0, it is easy to make sure, that the spiralities of lepton and quark should be sowed separately in subprocess $l^{-}+q\Rightarrow l^{-}+q$. That's why in this process onlu four spiral amplitudes F_{LL}, F_{LR}, F_{RL} and F_{RR}, which describe following reactions:

$$\begin{aligned} &l_L^{-}+q_L\Rightarrow l_L^{-}+q_L\,, \quad l_L^{-}+q_R\Rightarrow l_L^{-}+q_R \\ &l_R^{-}+q_L\Rightarrow l_R^{-}+q_L\,, \quad l_R^{-}+q_R\Rightarrow l_R^{-}+q_R\,. \end{aligned} \quad (10)$$

The spiral amplitudes in SM are defined by expressions

$$F_{\alpha\beta}=\frac{Q_q}{xys}-\frac{g_{\alpha}^{l}g_{\alpha}^{q}}{xys+M_Z^2}, \qquad (\alpha,\beta=L;R)\,, \quad (11)$$

where M_Z – is mass of Z^0-bozon, $\sqrt{s}$ – is the total energy, in the initial lepton=proton c.m.frame, Q_q is quark electric charge, g_R^l and g_L^l (g_R^q and g_L^q) are right and left neutral weak charges of lepton (quark) with Z^0-bozon:

$$g_R^l = \sqrt{\frac{x_w}{1-x_w}}\ ,\ g_L^l = \frac{-1/2 + x_w}{\sqrt{x_w(1-x_w)}}\ ;$$
$$g_R^q = -Q_q\sqrt{\frac{x_w}{1-x_w}}\ ,\ g_L^q = \frac{T_3 - Q_q x_w}{\sqrt{x_w(1-x_w)}}\ . \qquad (12)$$

Here $x_w = \sin^2\theta_w$ – is the Weinberq's parameter, T_3 is third projection of the weak isospin of quark q.

The differential cross-section of the elementary subprocess $l^- q \Rightarrow l^- q$ with taking under the consideration of the spiralities of the initial units can be imagined in the from (the spiralities of the final particles are the same, as of the initial ones, i.e. the spiralities of lepton and quark are saved separately):

$$\frac{d\hat{\sigma}}{dy} = \pi\alpha^2 xs\{(1+\lambda)(1+h_q)F_{RR}^2 + (1-\lambda)(1-h_q)F_{LL}^2 +$$
$$+ (1-y)^2\left[(1+\lambda)(1-h_q)F_{RL}^2 + (1-\lambda)(1-h_q)F_{LR}^2\right]\}, \qquad (13)$$

where h_q is spirality of the initial quark.

The differential cross-section of subprocess $l^-\bar{q} \Rightarrow l^-\bar{q}$ can be obtained from (13) with the help of the elementary changes: $F_{RR} \Leftrightarrow F_{RL}$, $F_{LL} \Leftrightarrow F_{LR}$.

On the base of formulas (9) and (13), the expression for the differential cross-section of semi-inclusive reaction $l^- N \Rightarrow l^- hX$ has been obtained [6,7]:

$$\frac{d\sigma^-(\lambda;h_N)}{dxdydz} = 2\pi\alpha^2 sx\sum_q\{f_q^N(x,Q^2)D_q^h(z,Q^2)f_1 + f_{\bar{q}}^N(x,Q^2)D_{\bar{q}}^h(z,Q^2)f_2 +$$
$$+ h_N\left[\Delta f_q^N(x,Q^2)D_q^h(z,Q^2)f_3 + \Delta f_{\bar{q}}^N(x,Q^2)D_{\bar{q}}^h(z,Q^2)f_4\right]\}, \qquad (14)$$

where

$$f_{\substack{1\\3}} = (1+\lambda)\left[F_{RR}^2 \pm (1-y)F_{RL}^2\right] \pm (1-\lambda)\left[F_{LL}^2 \pm (1-y)^2 F_{LR}^2\right],$$
$$f_{\substack{2\\4}} = (1+\lambda)\left[F_{RL}^2 \pm (1-y)^2 F_{RR}^2\right] \pm (1-\lambda)\left[F_{LR}^2 \pm (1-y)^2 F_{LL}^2\right], \qquad (15)$$
$$f_q^N(x,Q^2) = f_{q(+1)}^{N(+1)}(x,Q^2) + f_{q(-1)}^{N(+1)}(x,Q^2)\ ,$$
$$\Delta f_q^N(x,Q^2) = f_{q(+1)}^{N(+1)}(x,Q^2) + - f_{q(-1)}^{N(+1)}(x,Q^2).$$

The differential cross=section of process $l^+ N \Rightarrow l^+ hX$ must be obtained from (14) with the help of the following exchanges:

$$F_{R\beta} \Leftrightarrow F_{L\beta}\ (\beta = R;\ L).$$

We can now compute the so called "difference double spin asymmetry" $A_N^{h^+-h^-}$ which is expressed as

$$A_N^{h^+-h^-} = \frac{(\sigma_{\uparrow\uparrow}^{h^+} - \sigma_{\uparrow\uparrow}^{h^-}) - (\sigma_{\uparrow\downarrow}^{h^+} - \sigma_{\uparrow\downarrow}^{h^-})}{(\sigma_{\uparrow\uparrow}^{h^+} - \sigma_{\uparrow\uparrow}^{h^-}) + (\sigma_{\uparrow\downarrow}^{h^+} - \sigma_{\uparrow\downarrow}^{h^-})}, \qquad (16)$$

Where denotes the cross-sections (14) with parallel (antiparalel) orientations of the lepton and target nuclear spins. Then, the expression for the double spin asymmetries look like:

$$A_p^{\pi^+-\pi^-} = \{\Delta u_v\left[F_{LL}^2(u)-(1-y)^2F_{LR}^2(u)\right]-\Delta d_v\left[F_{LL}^2(d)-(1-y)^2F_{LR}^2(d)\right]+$$
$$+\left[1+(1-y)^2\right]\left[\Delta u_s(F_{LL}^2(u)-F_{LR}^2(u))-\Delta d_s(F_{LL}^2(d)-F_{LL}^2(d))\right]\}\times$$
$$\times\{u_v\left[F_{LL}^2(u)+(1-y)^2F_{LR}^2(u)\right]-d_v\left[F_{LL}^2(d)+(1-y)^2F_{LR}^2(d)\right]+$$
$$+\left[1-(1-y)^2\right]\left[u_s(F_{LL}^2(u)-F_{LR}^2(u))-d_s(F_{LL}^2(d)-F_{LL}^2(d))\right]\}^{-1}\ ; \qquad (17)$$

$$A_p^{K^+-K^-} = \{\Delta u_v\left[F_{LL}^2(u)-(1-y)^2F_{LR}^2(u)\right]+$$
$$+\left[1+(1-y)^2\right]\left[\Delta u_s(F_{LL}^2(u)-F_{LR}^2(u))-\Delta s_s(F_{LL}^2(s)-F_{LR}^2(s))\right]\}+$$
$$+\{u_v\left[F_{LL}^2(u)+(1-y)^2F_{LR}^2(u)\right]+$$
$$+\left[1-(1-y)^2\right]\left[u_s(F_{LL}^2(u)-F_{LR}^2(u))-s_s(F_{LL}^2(s)-F_{LL}^2(s))\right]\}^{-1}, \qquad (18)$$

where u_v and d_v(u_s , d_s , s_s) are distribution functions valence *u-* and *d- (sea u-, d-, s-)* (quarks) in proton.

The double spin asymmetries (17) and (18) have the remarkable property – they to be free of any fragmentation functions. When we do not consider weak interaction contributions in the processes $l^-N \Rightarrow l^-hX$ expressions for the difference asymmetries look like:

$$A_p^{\pi^+-\pi^-} = f(y)\cdot\frac{4\Delta u_v-\Delta d_v}{4u_v-d_v}\ ,$$
$$A_n^{\pi^+-\pi^-} = f(y)\cdot\frac{4\Delta d_v-\Delta u_v}{4d_v-u_v}\ ,$$
$$A_p^{K^+-K^-} = f(y)\cdot\frac{\Delta u_v}{u_v}\ , \qquad (19)$$
$$A_n^{K^+-K^-} = f(y)\,\frac{\Delta d_v}{d_v}\ ,$$
$$A_d^{\pi^+-\pi^-} = A_d^{K^+-K^-} = f(y)\frac{\Delta u_v+\Delta d_v}{u_v+d_v}\ ,$$
$$f(y)=\frac{1-(1-y)^2}{1+(1-y)^2}\ .$$

The double-spin asymmetries (19) contain only valence quark polarized densities.

2. Neutral current neutrino processes $\nu_\mu\ (\bar\nu_\mu)N \Rightarrow \nu_\mu\ (\bar\nu_\mu)\,hX$

There are two kinds of elementary interactions contributing to these processes

$$\begin{aligned}\nu_\mu\ (\bar\nu_\mu)+q &\Rightarrow \nu_\mu\ (\bar\nu_\mu)+q\,,\\ \nu_\mu\ (\bar\nu_\mu)+q &\Rightarrow \nu_\mu\ (\bar\nu_\mu)+\bar q.\end{aligned} \qquad (20)$$

As quarks spirality conserves in neglect of its masses, then the elementary subprocees $\nu_\mu + q \Rightarrow \nu_\mu + q$ is defined only by two spiral amplitudes F_{LL} and F_{LR}, which describe following reactions:

$$\nu_L + q_L \Rightarrow \nu_L + q_L, \qquad \nu_L + q_R \Rightarrow \nu_L + q_R. \qquad (21)$$

The spiral amplitudes in SM are defined by following expressions

$$F_{LL} = \frac{g_L^v g_L^q}{xys+M_Z^2}\ , \qquad F_{LR} = \frac{g_L^L g_R^q}{xys+M_Z^2}\ , \qquad (22)$$

where

$$g_L^v = \frac{1}{2}\cdot\frac{1}{\sqrt{x_w(1-x_w)}}\ .$$

The differential cross-section of the elementary subprocess $\nu_\mu + q \Rightarrow \nu_\mu + q$ taking into consideration the spirality of initial quarks h_q can be presented in the form

$$\frac{d\sigma}{dy} = 2\pi\alpha^2 xs\left[\left(1-h_q\right)F_{LL}^2+\left(1+h_q\right)(1-y)^2F_{LR}^2\right]. \qquad (23)$$

The following expression has been obtained on the base of formulas (9) and (23), for the differential cross-section of semi-inclusive reaction $\nu_\mu N \Rightarrow \nu_\mu hX$:

$$\frac{d\sigma}{dxdydz} = \pi\alpha^2 xs\sum_q\{f_q^N(x,Q^2)D_q^h(z,Q^2)\left[F_{LL}^2+(1-y)^2F_{LR}^2\right]+f_{\bar q}^N(x,Q^2)D_{\bar q}^h(z,Q^2)\times$$
$$\times\left[F_{LR}^2+(1-y)^2F_{LL}^2\right]-h_N\Delta f_q^N(x,Q^2)\,D_q^h(x,Q^2)\left[F_{LL}^2-(1-y)^2F_{LR}^2\right]-$$
$$-h_N\Delta f_{\bar q}^N(x,Q^2)\,D_{\bar q}^h(z,Q^2)\left[F_{LR}^2-(1-y)^2F_{LL}^2\right]\}, \qquad (24)$$

The double spin asymmetries for the semi-inclusive reactions $\nu_\mu p \Rightarrow \nu_\mu \pi^\pm X$ and $\nu_\mu p \Rightarrow \nu_\mu K^\pm X$ similarly *Eqs* (17) and (18).

3. Charged current processes $\nu_\mu(\bar{\nu}_\mu)N \Rightarrow \mu^-(\mu^+)hX,\ \mu^-(\mu^+)N \Rightarrow \nu_\mu(\bar{\nu}_\mu)hX$.

Let us consider the neutrino initiated processes $\nu_\mu N \Rightarrow \mu^- hX$: for them there exist four possible elementary contributions:

$$\begin{aligned} &\nu_\mu + d \Rightarrow \mu^- + u, \quad \nu_\mu + s \Rightarrow \mu^- + u, \\ &\nu_\mu + \bar{u} \Rightarrow \mu^- + \bar{d}, \quad \nu_\mu + \bar{u} \Rightarrow \mu^- + \bar{s}. \end{aligned} \tag{25}$$

There is only one non-zero helicity amplitude for each of the elementary processes in (25):

$$F_{LL} = \frac{1}{xys + M_w^2} \cdot \frac{U_{qq'}}{x_w}, \tag{26}$$

where $U_{ud} = \cos\theta_c$, $U_{uc} = \sin\theta_c$, θ_c is the Cabibbo angle, M_w is the mass of W - boson.

The differential cross-section of semi-inclusive reaction $\nu_\mu N \Rightarrow \mu^- hX$ must be written in the following form:

$$\begin{aligned} \frac{d\sigma}{dxdydz} = \frac{\pi\alpha^2}{2} xs \sum_{q,q'} \{ & F_{LL}^2(x,Q^2) D_{q'}^h(z,Q^2) + (1-y)^2 \cdot f_{\bar{q}}^N(x,Q^2) D_{\bar{q}'}^h(z,Q^2) - \\ & - h_N \left[\Delta f_q^N(x,Q^2)\, D_{q'}^h(x,Q^2) - (1-y)^2 \Delta f_{\bar{q}}^N(x,Q^2)\, D_{\bar{q}'}^h(z,Q^2) \right] \}. \end{aligned} \tag{27}$$

If we explicitly perform the sum over flavours in the numerators and denominators of *Eqs.* (16), we obtain for double-spin asymmetries:

$$A_p^{\pi^+ - \pi^-}(\nu_\mu p) = \frac{\Delta d_v + \Delta d_s(1+R) - (1-y)^2 \Delta \bar{u}_s}{d_v + d_s(1+R) + (1-y)^2 \bar{u}_s}, \tag{28}$$

$$A_p^{K^+ - K^-}(\nu_\mu p) = \frac{\Delta d_v + \Delta d_s(1+R) - (1-y)^2 \Delta \bar{u}_s \cdot R}{d_v + d_s(1+R) + (1-y)^2 \bar{u}_s \cdot R}, \tag{29}$$

$$A_p^{\pi^+ - \pi^-}(\bar{\nu}_\mu p) = -\frac{(1-y)^2[\Delta u_v + \Delta u_s] - \Delta \bar{d}_s(1+R)}{(1-y)^2[u_v + u_s] + \bar{d}_s(1+R)}, \tag{30}$$

$$A_p^{K^+ - K^-}(\bar{\nu}_\mu p) = -\frac{(1-y)^2[\Delta u_v + \Delta u_s]R - \Delta \bar{d}_s(1+R)}{(1-y)^2[u_v + d_v] + \bar{d}_s(1+R)}, \tag{31}$$

where $R = tg^2\theta_c = 0{,}056$.

Similar results hold for the $\mu^- p \Rightarrow \nu_\mu hX$ and $\mu^+ p \Rightarrow \bar{\nu}_\mu hX$ processes; the contributing elementary interactions are:

$$\begin{aligned} &\mu^- + u \Rightarrow \nu_\mu + d, \quad \mu^- + u \Rightarrow \nu_\mu + s, \\ &\mu^- + \bar{d} \Rightarrow \nu_\mu + \bar{u}, \quad \mu^- + \bar{s} \Rightarrow \nu_\mu + \bar{u}, \\ &\mu^+ + d \Rightarrow \bar{\nu}_\mu + u, \quad \mu^+ + s \Rightarrow \bar{\nu}_\mu + u, \\ &\mu^+ + \bar{u} \Rightarrow \bar{\nu}_\mu + \bar{d}, \quad \mu^+ + \bar{u} \Rightarrow \bar{\nu}_\mu + \bar{s}. \end{aligned} \tag{32}$$

The analogues of *Eqs*. (28)-(31) are now [8]:

$$A_p^{\pi^+-\pi^-}(\mu^- p) = \frac{\Delta u_v + \Delta u_s - (1-y)^2 \Delta \bar{d}_s (1+R)}{u_v + u_s + (1-y)^2 \bar{d}_s (1+R)}\ , \tag{33}$$

$$A_p^{K^+-K^-}(\mu^- p) = \frac{(\Delta u_v + \Delta u_s) R - (1-y)^2 \Delta \bar{d}_s (1+R)}{(u_v + u_s) R + (1-y)^2 \bar{d}_s (1+R)}\ , \tag{34}$$

$$A_p^{\pi^+-\pi^-}(\mu^+ p) = \frac{\Delta \bar{u}_s - (1-y)^2 [\Delta d_v + \Delta d_s (1+R)]}{u_s + (1-y)^2 [d_v + d_s (1+R)]}\ , \tag{35}$$

$$A_p^{K^+-K^-}(\mu^+ p) = \frac{\Delta \bar{u}_s R - (1-y)^2 [\Delta d_v + \Delta d_s (1+R)]}{u_s R + (1-y)^2 [d_v + d_s (1+R)]}\ . \tag{36}$$

4. Numerical estimates

In the previous sections we have obtained explicit expressions for the double-spin asymmetries for hadron production in semi-inclusive DIS. We now use these formulae to give prediction in the case of $\pi^{\pm}$ and $K^{\pm}$ production. The double-spin asymmetry values depend on the known SM dynamics, on the quark distribution functions in nucleons are present in references [9-12]. The distribution functions of valence and sea polarized quarks in nucleons, mentioned in ref. [9] are used bu us for the numerical estimations of double-spin asymmetries.

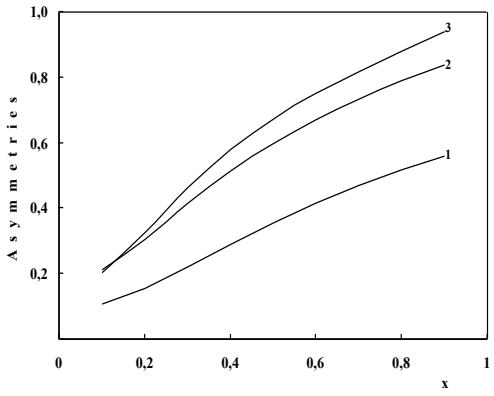

Fig. 1. The double-spin asymmetry $A_p^{\pi^+-\pi^-}$ for the pion production $ep \Rightarrow e\pi^{\pm}X$, as a function *x*, for different values *y*: *y=0.1* (*line 1*), *y=0.4* (*line 2*), *y=0.3* (*line 3*).

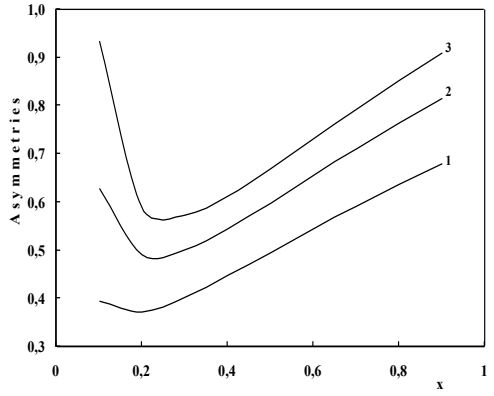

Fig. 2. The double-spin asymmetry $A_p^{K^+-K^-}$ for the kaon production $v_\mu p \Rightarrow v_\mu K^{\pm} X$, as a function of *x*, at fixed *y=0.1* (*line 1*), *y=0.4* (*line 2*), *y=0.7* (*line 3*).

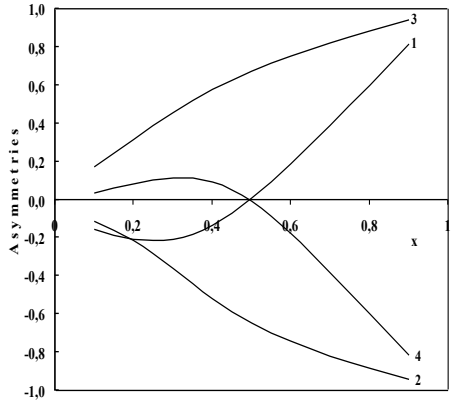

Fig. 3. The double-spin asymmetry $A_p^{\pi^+-\pi^-}$ as a function *x*, at fixed *y=0,4* for $v_\mu p \Rightarrow \mu^- \pi^{\pm} X$ (*line 1*), $v_\mu p \Rightarrow \mu^+ \pi$ (*line 2*), $\mu^- p \Rightarrow v_\mu \pi^{\pm} X$ (*line 3*) and $\mu^+ p \Rightarrow \bar{v}_\mu \pi^{\pm} X$ (*line 4*).

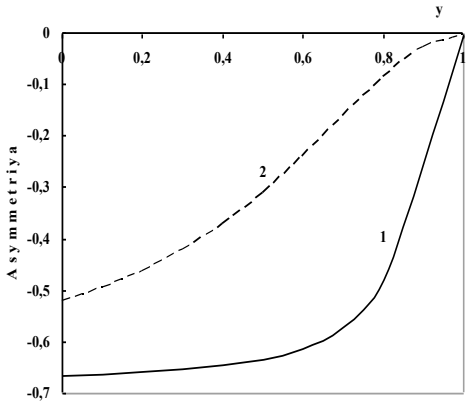

Fig. 4. The double-spin asymmetry $A_p^{h^+-h^-}$ as a function y, at fixed x=0,5 for $\bar{v}_\mu p \Rightarrow \mu^+ \pi^{\pm} X$ (*line 1*) and $\bar{v}_\mu p \Rightarrow \mu^+ K^{\pm} X$ (*line 2*).

In Fig. 1 we give - dependence of asymmetry $A_p^{\pi^+-\pi^-}$ in semi-inclusive reaction $e^- p \Rightarrow e^- \pi^{\pm} X$ at energy $\sqrt{s} = 300 GeV$ (ep-collider HERA), Weinberg parameter $x_w=0.232$ and the fixed value *y=0.1* (*line 1*), *y=0.4* (*line 2*), *y=0.9* (*line 3*). As it is seen the double-spin

asymmetry $A_p^{\pi^+-\pi^-}$ is positive and increase monotonously with increase of x.

The Fig. 2 illustrates the dependence of double-spin asymmetry $A_p^{K^+-K^-}$ in $\nu_\mu + p \Rightarrow \nu_\mu + K^\pm + X$ process on x at *y=0.1* (*line 1*), *y=0.4* (*line 2*), *y=0.7* (*line* 3).

The double-spin asymmetries $A_p^{\pi^+-\pi^-}$ and $A_p^{K^+-K^-}$ for charge currents are shown in Figs. 3 and 4.

[1] *C. Adloff* et al., Z. Phys., C 74 (1997), 191.
[2] *Wagner.* Tr. J. of Physics, 22 (1998), 525.
[3] *Airapetian et al.*, Phys. Lett., B 535 (2002), 85.
[4] *Aiaopetian et al.*, Phys. Rev., D71 (2005), 0122003.
[5] *K. Abe et al.,* Phys. Rev., Lett., 79 (1997), 26.
[6] *S.K.Abdullayev, A.I. Mukhtarov, M.Sh. Gojayev,* Azerbaijan Journal of Phys., Fizika, V. XVI, N. 3-4 (2010), 70.
[7] *S.K. Abdullayev, A.I. Mukhtarov, M.Sh. Gojayev,* Azerbaijan Journal of Phys., Fizika, V. XVIII, N. 1(2012), 7.
[8] *S.Q. Abdullayev,* Bakı Universitetinin xəbərləri, fizika-riyaziyyat elmləri seriyası, N. 2 (2013), 106.
[9] *H.Y. Cheng, S.N. Lai, C.Y. Wu.* Phys. Rev. D 53 (1996), 2380.
[10] *M. Hirari, S. Kumano, N. Saito,* Phys. Rev. D 69 (2004), 054021.
[11] *D.De florian, M. Stratman, W. Vogelsand,* Phys. Rev. D 57 (1998), 5811.
[12] *A.D. Martin* et. al., ar : 0901. 0002 v. 3 [hep-ph] (2009).

Received: 10.09.2013

THE POLARIZATION OF B-BARYON IN SEMI-INCLUSIVE REACTIONS

S.K. ABDULLAYEV, M.Sh. GOJAYEV
Baku State University, Az-1148, Z.Khalilov str., 23
S_abdullayev@mail.ru

Semi-inclusive reactions $e^{\pm}N \Rightarrow e^{\pm}BX$, $\nu_{\mu}(\bar{\nu}_{\mu})N \Rightarrow \nu_{\mu}(\bar{\nu}_{\mu})BX$, $\nu_{\mu}(\bar{\nu}_{\mu})N \Rightarrow \mu^{-}(\mu^{+})BX$, $\mu^{-}(\mu^{+})N \Rightarrow \nu_{\mu}(\bar{\nu}_{\mu})BX$ are studies in the framework of Standard model. The expression for polarization of B -bayron are obtained.

Keywords: Nuclear physics, B-Baryon
PACS: 95.30.Cq.

High energy experiment with polarized beams and targets has opened a new window for revealing QCD dynamics and hadron structures. Ongoing RHIC-SPIN, HERMES and COMPASS experiments are going to provide us with a variety of data disclosing spin distribution inside the nucleon. The Electron Ion Collider (EIC) at BNL is expected to be a more powerful and sensitive tool for the QCD spin physics. In this paper, we study the longitudinally polarized boryons production in semi-inclusive deep inelastic (DIS) off nucleon (they are intensive investigated experimentally at the present time [1-5].

$$l^{\pm} + N \Rightarrow l^{\mp} + B(h_B) + X\,, \qquad (1)$$

$$\nu_{\mu}(\bar{\nu}_{\mu}) + N \Rightarrow \nu_{\mu}(\bar{\nu}_{\mu}) + B(h_B) + X\,, \qquad (2)$$

$$\nu_{\mu}(\bar{\nu}_{\mu}) + N \Rightarrow \mu^{-}(\mu^{+}) + B(h_B) + X\,, \qquad (3)$$

$$\mu^{-}(\mu^{+}) + N \Rightarrow \nu_{\mu}(\bar{\nu}_{\mu}) + B(h_B) + X\,, \qquad (4)$$

where h_B is the longitudinal polarization of B -baryon.

The cross-section for the production of a B -baryon in the current fragmentation region are given by

$$\frac{d\sigma(h_B)}{dxdydz} = \sum_{q,h_q} f_q^N(x) \frac{d\hat{\sigma}}{dy} D_{q(h_q)}^{B(h_B)}(z), \qquad (5)$$

where $f_q^N(x)$ is the distribution functions of quarks in the nucleon, $D_{q(h_q)}^{B(h_B)}(z)$ is the fragmentation functions of the polarized quarks to the polarized B -baryon, $\frac{d\hat{\sigma}}{dy}$ is the elementary cross-section. The usual DIS variables x, y and z defined as:

$$x = \frac{Q^2}{2P\cdot q}, \qquad y = \frac{q\cdot P}{P\cdot k}, \qquad z = \frac{P_B\cdot P}{P\cdot q},$$

where k, P, P_B and q are the four moments of the initial lepton, the target nucleon, the B-baryon and the virtual boson correspondingly.

Let us consider first the processes $l^{\mp}N \Rightarrow l^{\mp}BX$; for them there exist two possible elementary contributions

$$l^{\mp} + q \Rightarrow l^{\mp} + q\,,\ l^{\mp} + \bar{q} \Rightarrow l^{\mp} + \bar{q}\,.$$

Taking under the considerations the exchange of γ and Z^0, it is easy to make sure, that the spiralities of lepton and quark should be saved separately in subprocess $l^{-} + q \Rightarrow l^{-} + q$. That's why in this process is defined by only four spiral amplitudes F_{LL}, F_{LR}, F_{RL} and F_{RR}, which describe following reactions:

$$l_L^- + q_L \Rightarrow l_L^- + q_L,$$
$$l_L^- + q_R \Rightarrow l_L^- + q_R,$$
$$l_R^- + q_L \Rightarrow l_R^- + q_L,$$
$$l_R^- + q_R \Rightarrow l_R^- + q_R.$$

The spiral amplitudes in standard model (SM) are defined by expressions

$$F_{\alpha\beta} = \frac{Q_q}{xys} - \frac{g_{\alpha}^{l} g_{\beta}^{q}}{xys + M_Z^2}\,, \quad (\alpha,\beta = L;R) \qquad (6)$$

where M_Z -is mass of Z^0-bozon, $\sqrt{s}$ – is the energy of the lN -system in their c.m.s., Q_q is quark electric charge, g_R^l and g_L^l (g_R^q and g_L^q) are right and left neutral weak charges of lepton (quark) with Z^0-boson:

$$g_R^l = \sqrt{\frac{x_w}{1-x_w}}\,,\ g_L^l = \frac{-1/2 + x_w}{\sqrt{x_w(1-x_w)}}\,;$$
$$g_R^q = -Q_q\sqrt{\frac{x_w}{1-x_w}}\,,\ g_L^q = \frac{T_3 - Q_q x_w}{\sqrt{x_w(1-x_w)}}\,. \qquad (7)$$

Here $x_w = \sin^2\theta_w$ - is the Weinberq's parameter, T_3 is third projection of the weak isospin of quark q .

The differential cross-section of the elementary subprocess $l^{-}q \Rightarrow l^{-}q$ with taking under the consideration of the spirality of the final quark can be imagined in the from

$$\frac{d\hat{\sigma}}{dy}=\pi\alpha^2 xs\left\{(1+h_q)[F_{RR}^2+(1-y)^2\ F_{LR}^2]+\ (1-h_q)\left[F_{LL}^2+(1-y)^2\ F_{RL}^2\right]\right\}. \quad (8)$$

The differential cross-section of subprocess $l^-\bar{q}\Rightarrow l^-\bar{q}$ can be obtained from (8) with the help of the elementary changes: $F_{RR}\Leftrightarrow F_{RL}$, $F_{LL}\Leftrightarrow F_{LR}$.

On the base of formulas (5) and (8), the expression for the differential cross-section of semi-inclusive reaction $l^-N\Rightarrow l^-BX$ has been obtained [6,7]:

$$\begin{aligned}\frac{d\sigma^-(h_B)}{dxdydz}=\pi\alpha^2 sx\sum_q\Big\{&f_q^N(x)D_q^h(z)[F_{RR}^2+F_{LL}^2+(1-y)^2(F_{RL}^2+F_{LR}^2)]+\\&+f_{\bar{q}}^N(x)D_{\bar{q}}^B(z)\left[F_{RL}^2+F_{LR}^2+(1-y)^2(F_{RR}^2+F_{LL}^2)\right]+\\&+h_B\Big[f_q^N(x)\,\Delta D_q^B(z)\left(F_{RR}^2-F_{LL}^2-(1-y)^2(F_{RL}^2-F_{LR}^2)\right)+\\&+f_{\bar{q}}^N(x)\Delta D_{\bar{q}}^B(z)\left(F_{RL}^2-F_{LR}^2-(1-y)^2(F_{RR}^2-F_{LL}^2)\right)\Big]\Big\}\end{aligned} \quad (9)$$

where

$$D_q^B(z)=D_{q(+1)}^{B(+1)}(z)+\ D_{q(-1)}^{B(+1)}\ (z)\ ,$$
$$\Delta D_q^B(z)=D_{q(+1)}^{B(+1)}(z)-D_{q(+1)}^{B(+1)}\ (z).$$

The differential cross-section of semi-inclusive DIS antilepton on nucleon $l^+N\Rightarrow l^+BX$ can be obtained from (9) with the help of the following exchanges:

$$F_{RR}\Leftrightarrow F_{LR}\ ,\qquad F_{LR}\Leftrightarrow F_{LL}\ .$$

We can now compute the longitudinal polarizations $P_B^{(-)}$ and $P_B^{(+)}$ for B-baryon produced in lepton and antilepton initiated scattering processes:

$$P_B^{(\mp)}=\frac{d\sigma^{(\mp)}(h_B=1)-d\sigma^{(\mp)}(h_B=-1)}{d\sigma^{(\mp)}(h_B=1)+d\sigma^{(\mp)}(h_B=-1)} \quad (10)$$

The polarization of B-baryon is non-zero onlu due to parity violating weak contributions and we obtain (neglecting the contribution of antiquars):

$$P_B^{(-)}=\frac{\sum_q f_q^N(x)\Delta D_q^B(z)\left[F_{RR}^2-F_{LL}^2-(1-y)^2(F_{RL}^2-F_{LR}^2)\right]}{\sum_q f_q^N(x)D_q^B(z)\left[F_{RR}^2+F_{LL}^2+(1-y)^2(F_{RL}^2+F_{LR}^2)\right]}. \quad (11)$$

There are two different kinds of elementary interactions contributing to neutral current neutrino (antineutrino) processes $\nu_\mu\ (\bar{\nu}_\mu)N\Rightarrow\nu_\mu\ (\bar{\nu}_\mu)\ BX$:

$$\nu_\mu\ (\bar{\nu}_\mu)+q\Rightarrow\nu_\mu\ (\bar{\nu}_\mu)+q,$$
$$\nu_\mu\ (\bar{\nu}_\mu)+q\Rightarrow\nu_\mu\ (\bar{\nu}_\mu)+\bar{q}.$$

As quarks spirality conserves in neglect of its masses, then the elementary subprocess $\nu_\mu+q\Rightarrow\nu_\mu\ +q$ is defined only by two spiral amplitudes F_{LL} and F_{LR}, which describe following reactions:

$$\begin{matrix}\nu_L\ +q_L\Rightarrow\nu_L\ \ +q_L,\\ \nu_L\ +q_R\Rightarrow\nu_L\ \ +q_R\end{matrix}.$$

The spiral amplitudes in SM are defined by following expressions

$$F_{LR}=\frac{g_L^v g_R^q}{xys+M_Z^2},\quad F_{LL}=\frac{g_L^v g_L^q}{xys+M_Z^2}\ , \quad (12)$$

where

$$g_L^v=\frac{1}{2}\cdot\frac{1}{\sqrt{x_w(1-x_w)}}\ .$$

The differential cross-section of the elementary subprocess $\nu_\mu+q\Rightarrow\nu_\mu\ +\ q$ taking into consideration the spirality of final quark can be presented in the form:

$$\frac{d\hat{\sigma}}{dy}=\pi\alpha^2 xs\left[(1-h_q)F_{LL}^2+(1+h_q)(1-y)^2F_{LR}^2\right]. \quad (13)$$

The following expression has been obtained on the base of formulas (5) and (13) for the differential cross-section of semi-inclusive reaction $\nu_\mu N\Rightarrow\nu_\mu B+X$:

$$\frac{d\sigma(h_B)}{dxdydz} = \pi\alpha^2 xs\sum_q \{f_q^N(x)D_q^B(z)\left[F_{LL}^2 + (1-y)^2 F_{LR}^2\right] + f_{\bar{q}}^N(x)D_{\bar{q}}^B(z)\times$$
$$\times\left[F_{LR}^2 + (1-y)^2 F_{LL}^2\right] + h_B f_q^N(x)\Delta D_q^B(z)\left[(1-y)^2 F_{LR}^2 - F_{LL}^2\right] +$$
$$+ h_B f_{\bar{q}}^N(x)\Delta D_{\bar{q}}^B(z)\left[(1-y)^2 F_{LL}^2 - F_{LR}^2\right]\}, \quad (14)$$

Neglecting the contribution of antiquarks, we have take following expression for the longitudinal polarization degree of baryon:

$$P_B^{(\nu_\mu N)} = \frac{\sum_q f_q^N(x)\Delta D_q^B(z)\left[(1-y)^2(F_{LR}^2 - F_{LL}^2)\right]}{\sum_q f_q^N(x)D_q^B(z)\left[F_{LL}^2 + (1-y)^2 F_{LR}^2\right]} \quad (15)$$

Let us consider the neutrino initiated processes $\nu_\mu N \Rightarrow \mu^- BX$: for them there exist four possible elementary contributions:

$$\nu_\mu + d \Rightarrow \mu^- + u, \quad \nu_\mu + s \Rightarrow \mu^- + u,$$
$$\nu_\mu + \bar{u} \Rightarrow \mu^- + \bar{d}, \quad \nu_\mu + \bar{u} \Rightarrow \mu^- + \bar{s}. \quad (16)$$

Neglecting quarks masses one find that there is only one non-zero helicity amplitude for each of the elementary processes in (16):

$$F = \frac{1}{xys + M_w^2}\cdot\frac{U_{qq'}}{x_w}, \quad (17)$$

where $U_{ud} = \cos\theta_c$, $U_{uc} = \sin\theta_c$, θ_c is the Cabibbo angle, M_w is the mass of W - boson.

The differential cross-section of semi-inclusive processes $\nu_\mu N \Rightarrow \mu^- BX$ we have the following expression [8]:

$$\frac{d\sigma(h_B)}{dxdydz} = \frac{\pi\alpha^2 xs}{2}\sum_{q,q'} F^2\{f_q^N(x)D_{q'}^B(z) + (1-y)^2\cdot f_{\bar{q}}^N(x)D_{\bar{q}'}^B(z) -$$
$$- h_B\left[f_q^N(x)\Delta D_{q'}^B(z)(1-y)^2 - f_{\bar{q}}^N(x)\Delta D_{\bar{q}'}^B(z)\right]\}. \quad (18)$$

Summing on quark flavors for longitudinal polarization degree of baryon we have expression:

$$P_B^{(\nu_\mu\Rightarrow\mu^-)} = \frac{-(f_d^N(x) + Rf_s^N(x)\Delta D_u^B(z) + (1-y)^2 f_{\bar{u}}^N(x)(\Delta D_{\bar{d}}^B(z) + RD_{\bar{s}}^B(z))}{(f_d^N(x) + Rf_s^N(x))D_u^B(z) + (1-y)^2 f_{\bar{u}}^N(x)(\Delta D_{\bar{d}}^B(z) + RD_{\bar{s}}^B(z))} \quad (19)$$

$$P_B^{(\bar{\nu}_\mu\Rightarrow\mu^+)} = \frac{-f_u^N(x)(\Delta D_d^B(z) + RD_{\bar{s}}^B(z))(1-y)^2 + (f_{\bar{d}}^N(x) + Rf_{\bar{s}}^N(x))\Delta D_{\bar{u}}^B(z)}{f_u^N(x)(D_d^B(z) + RD_s^B(z))(1-y)^2 + (f_{\bar{d}}^N(x) + Rf_{\bar{s}}^N(x))D_{\bar{u}}^B(z)}, \quad (20)$$

where $R = tg^2\theta_c \approx 0.056$.

The formulae for longitudinal polarization degree (19), (20) are true in the case of creation of arbitrary B – baryon with spin 1/2. If we specify the final hadron observed, further simplifications are possible. Let's consider the case in with a Λ or $\Sigma^\pm$ baryon is produced. In this case we can neglect terms which contain both $\bar{q}$ distribution and $\bar{q}'$ fragmentation functions as they are both small, in particular at large x and z. Then we obtain the simple expression for longitudinal polarization degree of Λ -hyperon:

$$P_\Lambda^{(\nu_\mu\Rightarrow\mu^-)} = -\frac{\Delta D_u^\Lambda(z)}{D_u^\Lambda(z)}, \quad (21)$$

$$P_{\Lambda}^{(\bar{\nu}_{\mu}\Rightarrow\mu^{+})}=-\frac{\Delta D_{d}^{\Lambda}(z)+R\Delta D_{s}^{\Lambda}(z)}{D_{u}^{\Lambda}(z)+RD_{s}^{\Lambda}(z)} \qquad (22)$$

As it is seen, the longitudinal polarization of Λ^0-hyperon is only z function and doesn't depend on variables x and y. The study of this polarization can give the valuable information about fragmentation function on polarized quark to polarized baryon.

Similar results hold for the $\mu^{-}N\Rightarrow\nu_{\mu}BX$ and $\mu^{+}N\Rightarrow\bar{\nu}_{\mu}BX$ processes; the contributing elementary interactions are:

$$\mu^{-}+u\Rightarrow\nu_{\mu}+d,\quad \mu^{-}+u\Rightarrow\nu_{\mu}+s,$$
$$\mu^{-}+\bar{d}\Rightarrow\nu_{\mu}+\bar{u},\quad \mu^{-}+\bar{s}\Rightarrow\nu_{\mu}+\bar{u},$$
$$\mu^{+}+d\Rightarrow\bar{\nu}_{\mu}+u,\quad \mu^{+}+s\Rightarrow\bar{\nu}_{\mu}+u,$$
$$\mu^{+}+\bar{u}\Rightarrow\bar{\nu}_{\mu}+\bar{d},\quad \mu^{+}+\bar{u}\Rightarrow\bar{\nu}_{\mu}+\bar{s}.$$

The expressions for longitudinal polarization degree of baryon are simplified, if we can neglect the antiquark contribution in fragmentation functions:

$$P_{\Lambda}^{(\mu^{-}\Rightarrow\nu_{\mu})}=-\frac{\Delta D_{d}^{\Lambda}(z)+R\Delta D_{s}^{\Lambda}(z)}{D_{u}^{\Lambda}(z)+RD_{s}^{\Lambda}(z)}, \qquad (23)$$

$$P_{\Lambda}^{(\mu^{+}\Rightarrow\bar{\nu}_{\mu})}=-\frac{\Delta D_{u}^{\Lambda}(z)}{D_{u}^{\Lambda}(z)} \qquad (24)$$

The polarization values depend or the SM dynamics, on the quark distribution functions and on the quark fragmentation functions, both unpolarized and polarization. The later are not so well known and a choise must be made in order to give numerical estimates. In the literature there are set of distribution functions of quarks in nucleons [9-12].

The spin functions of quark fragmentation into Λ^0-hyperon are parametrized in form

$$\Delta D_{s}^{\Lambda}(z)=z^{\alpha}D_{s}^{\Lambda}(z),$$
$$\Delta D_{u}^{\Lambda}(z)=\Delta D_{d}^{\Lambda}(z)=N_{u}\Delta D_{s}^{\Lambda}(z)$$

and the parameter α and N_u are chosen in three variants

Parameter	Variant 1	Variant 2	Variant 3
α	0.62	0.27	1.66
N_u	0	-0.2	1

In Fig. 1-3 we show results for P_{Λ} for several processes, with different kinematical conditions. The Weinberg parameter $\sin^2\theta_w=0.232$ is given bu us.

The dependence of degree of longitudinal polarization of Λ^0- hyperon $P_{\Lambda}^{(-)}$ in reaction $e^{-}p\Rightarrow e^{-}\Lambda^{0}X$ at energy $\sqrt{s}=300\,GeV$ (ep-collider HERA) on x,y,z variables is given on the Fig. 1. As it is seen in 1 and 2 variants the degree of longitudinal polarization of Λ- hyperon is small and weakly depends on x,y,z variables.

In 3 variant polarization is negative and with the decrease of x,y,z, it weakly increase on module.

The analogical behavior is observed for $x-$, $y-$ and z-dependencies of polarization P_{Λ} in other semi-inclusive reactions, for example, the dependence of longitudinal polarization degree $P_{\Lambda}^{(\nu_{\mu}p)}$ and $P_{\Lambda}^{(\bar{\nu}_{\mu}p)}$ in $\nu_{\mu}p\Rightarrow\nu_{\mu}\Lambda^{0}X$ and $\bar{\nu}_{\mu}p\Rightarrow\bar{\nu}_{\mu}\Lambda^{0}X$ processes at the energy $\sqrt{s}=9.6\,GeV$ (experiment NOMAD in CERN) on x,y or z variables (the Figs. 2 and 3).

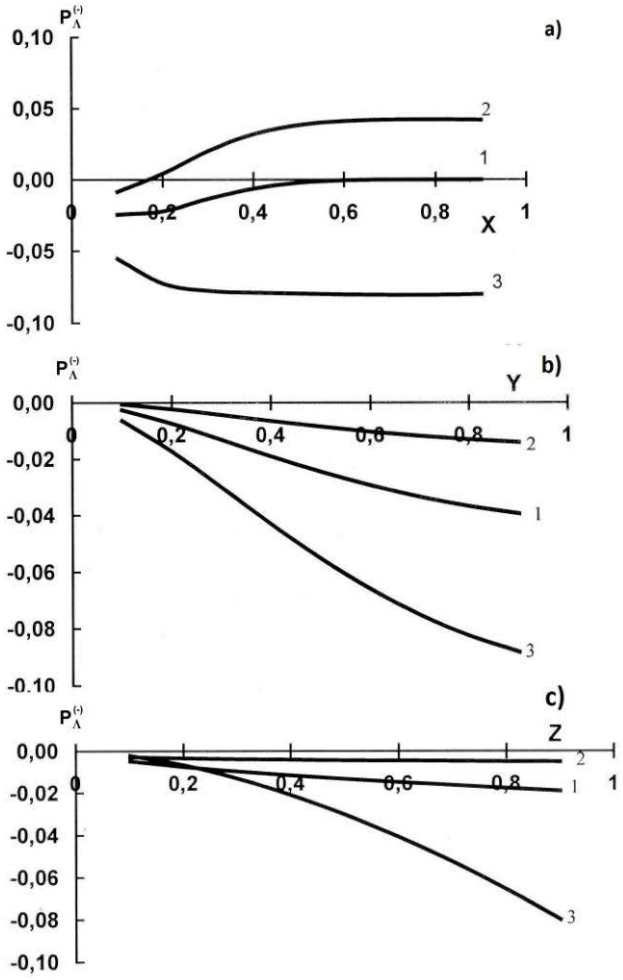

Fig. 1. The polarization $P_{\Lambda}^{(-)}$ for Λ^0-hyperon as a function of x at $y=z=0.5$ (a); of y at $x=0.1,\ z=0.5$ (b) and of z at $x=0.1,\ y=0.3$ (c)

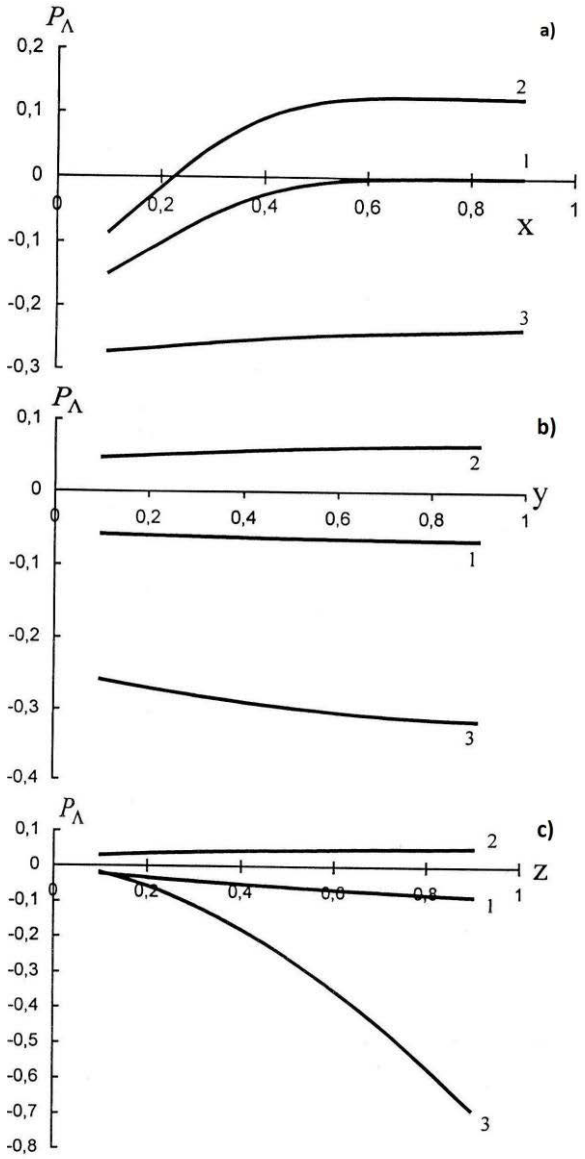

Fig. 2. The polarization $P_\Lambda^{(\nu_\mu p)}$ for Λ^0-hyperon in reaction $\nu_\mu p \Rightarrow \nu_\mu \Lambda^0 X$ as a function of x at $y = 0.1,\ z = 0.5\ (a)$; of y at $x = 0.3,\ z = 0.5\ (b)$ and of z at $x = 0.3,\ y = 0.1\ \ (c)$

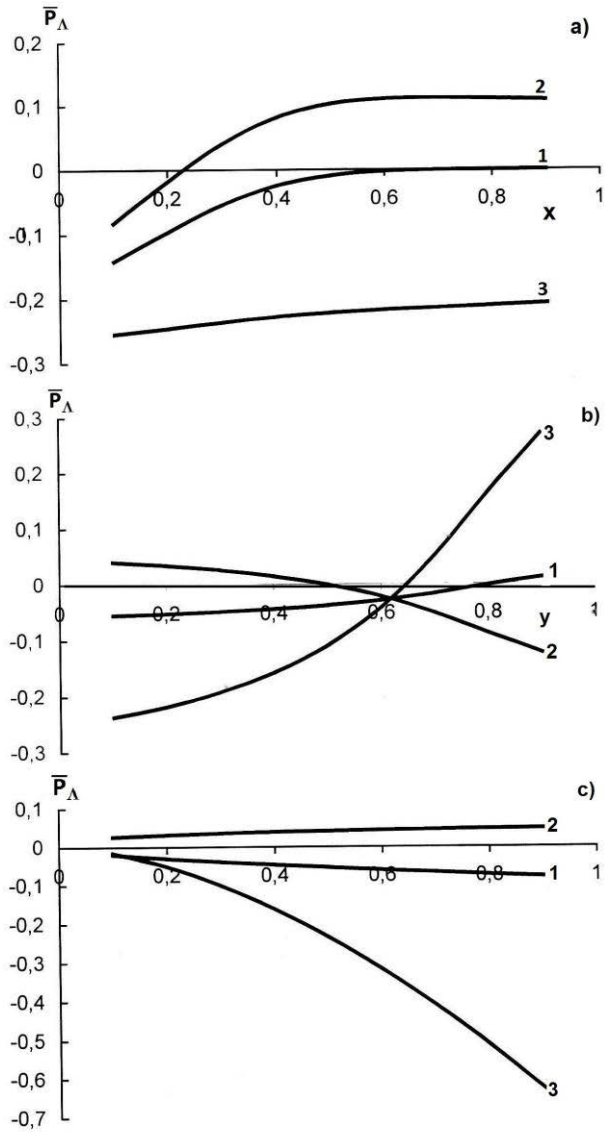

Fig.3. The polarization $P_\Lambda^{(\bar{\nu}_\mu p)}$ for Λ^0-hyperon in reaction $\bar{\nu}_\mu p \Rightarrow \bar{\nu}_\mu \Lambda^0 X$ as a function of x at $y = 0.1,\quad z = 0.5\ (a)$; of y at $x = 0.3,\ z = 0.5\ (b)$ and of z at $x = 0.3,\ y = 0.1\ \ (c)$

[1] *C. Adloff et al.,* Z. Phys., C 74 (1997), 191.
[2] *A. Wagner.* Tr. J. of Physics, 22 (1998), 525.
[3] *A. Airapetian et al.,* Phys. Lett., B 535 (2002), 85.
[4] *A. Airapetian et al*., Phys. Rev., D 71 (2005), 0122003.
[5] *K. Abe et al.,* Phys. Rev., Lett., 79 (1997), 26.
[6] *S.K. Abdullayev, A.I. Mukhtarov, M.Sh. Gojayev,* Azerbaijan Journal of Phys., Fizika, V. XVI, N. 3-4 (2010), 70.
[7] *S.K. Abdullayev, A.I. Mukhtarov, M.Sh. Gojayev*, Azerbaijan Journal of Phys., Fizika, V. XVIII, N. 1 (2012), 7.
[8] *S.Q. Abdullayev*, Bakı Universitetinin xəbərləri, fizika-riyaziyyat elmləri seriyası, N. 2 (2013), 106.
[9] *H.Y. Cheng, S.N. Lai, C.Y. Wu.* Phys. Rev. D 53 (1996), 2380.
[10] *M. Hirari, S. Kumano, N. Saito*, Phys. Rev. D 69 (2004), 054021.
[11] *D.De florian, M. Stratman, W. Vogelsand*, Phys. Rev. D 57 (1998), 5811.
[12] *A.D. Martin et. al*., ar : 0901. 0002 v. 3 [hep-ph] (2009).

Received: 11.09.2013

OPTICAL PARAMETERS OF BINARY COMPOUNDS $YbBi_2Te_4$ AND $YbBi_4Se_7$

N.Z. JALILOV, G.M. DAMIROV, M.A. MAKHMUDOVA
Institute of Physics
Of National Academy of Sciences
AZ-1143, H.Javid ave.,33, Baku Azerbaijan

The reflection coefficients of R(E) of $YbBi_2Te_4$ and $YbBi_4Se_7$ samples in interval of beam energy 1-6 eV incidenting normally on the surface are measured. The optical parameters of given compounds: dielectric constants (ε_1, ε_2), electro-optical differential functions (α,β), effective number of valence electrons $n_{eff}(E)$, defined by volume -Im(ε^{-1}) and surface -Im(1+ ε)$^{-1}$ electron losses, taking part in transitions, are defined with the help of Kramers-Kroning relations.

Keywords: dispersion, optical parameters, binary compounds.
PACS: 535.3; 539.2/6:539./.04

INTRODUCTION

The compounds of rare-earth elements are of great scientific and practical importance among triple compounds having the whole complex of interesting physical properties. The semiconductors and superconductor having the good luminescent characteristics and also compounds which are perspective ones for preparation of thermo-sensitive resistances and thermo-couples, gauges in remote control devices by thermal processes are found in these materials.

Binary compounds of rare-earth elements with partial and totally filled 4-f level of Ln_3X_4 and Ln_5X_7 types first of all presents scientific-theoretical interest because of unpaired number of valence electrons; they are the ten per anion, i.e. on one electron more than in usual total-valence semiconductor compounds. That's why the conduction of the given compounds isn't directly follows from general theory of valence bond. In semiconductors the one of bound atoms should have the occupation of s- and p-orbitals in valence membrane; the total occupation of these orbitals can take place only in elements of IV and VII groups of periodical system. The complex character of d- and f-electrons participation in bond, the bond radius of transition elements in crystals, overlapping of d-and f-atomic wave functions, the position of d-and f-bands in energy spectrum and etc differ the transition elements from compounds of s-and p-elements. $YbBi_2Te_4$ and $YbBi_4Se_7$ materials are the analogues of Ln_3X_4 and Ln_5X_7 [1]. The optical spectra $YbBi_2Te_4$ и $YbBi_4Se_7$ are investigated in the given work. The optical spectra of semiconductors are connected with their electron structures. The material energy level defining their many physicochemical properties is the one of its main parameters. The material dispersion knowledge allows us to forecast the principal possibilities of carrying out of definite properties and its application in semiconductor electronics.

The optical spectra of $YbBi_2Te_4$ and $YbBi_4Se_7$ aren't studied. The obtaining and investigation of optic parameter investigation of $YbBi_2Te_4$ and $YbBi_4Se_7$ is the aim of the work.

EXPERIMENTAL TECHNIQUE

The synthesis of $YbBi_2Te_4$ and $YbBi_4Se_7$ is carried out like as compound synthesis of $LnBi_2S_4(Se_4,Te_4)$, $LnBi_4S_7(Se_7,Te_7)$ type. The synthesis is carried out by the given types, mainly from bismuth elements of B-3 purity, ytterbium of Itb-1 type, selenium of B-5 type, tellurium of B-3 type by ampoule method or by binary compound melting. The synthesis of the given by us materials is carried out from elements by ampoule method. The ampoule length is 150 mm and diameter is 20mm. The synthesis is carried out in evacuated up to (~10^{-2}Pa) quartz ampoules at temperature 900-1200K in the dependence on the composition. After synthesis finishing the homogenizing annealing is carried out during 200h at temperature on 100^{0}C below than final crystallization one.

As it is mentioned in [2] the split YbTe-Bi_2Te_3 is quazi-binary; two compounds $YbBi_2T_4$ and $YbBi_4Te_7$ crystallize in the system. The split liquidus consists of branches of primary crystallization of YbTe, $YbBi_2Te_4$, $YbBi_4Te_7$, α – solid solutions on bismuth telluride base.

$YbBi_2Te_4$ compounds forms by peritectic reaction ж+ YbTe⇔$YbBi_2Te_4$ at temperature 873K. It is established that $YbBi_2Te_4$ has the polymorphic modifications: α-$YbBi_2Te_4$ at temperature 673K transits into β-$YbBi_2Te_4$.

As it is shown in works [3,4] $YbBi_2Te_4$ compound is isostructural one to $YbSb_2Te_4$ and has the cubic lattice of Th_3P_4 type with elementary cell parameter a=10,48±0,01A, d_{ex}=6,35gr/cm d_{cal}=6,40gr/cm^3, microhardness is H=1500 MPa. $YbBi_2Te_4$ compound is semiconductor with narrow forbidden band ΔE=0,34 eV.

$YbBi_4Se_7$ compound melts without decomposition at temperature 963K, it is dark grey color, and it is stable in air. Its density d=6,30gr/cm^3 and microhardness H=1660 MPa.

The structure of $YbBi_2Se_4$ and $YbBi_4Se_7$ compounds is studied on single crystals [5]. The structure of $YbBi_4Se_7$ compound is related to hexagonal syngony. The cell parameters are: a=13,90, c=14,384A, d_{ex}=7,45gr/cm, d_{cal}=7,5430 gr/cm^3. The electric conduction of $YbBi_4Se_7$ at 300K is ~$1{,}5\cdot10^{-4}$ Om$^{-1}\cdot$m^{-1} and forbidden gap ΔE = 0,81 eV.

The homogeneity region on the base of ytterbium monoselenide and triple compounds hasn't been studied.

The reflection coefficients of $YbBi_2Te_4$ and $YbBi_4Se_7$ are measured in normally to the surface incident beam energy interval 1-6eV.

The obtaining and investigation of optic parameter spectra $YbBi_2Te_4$ and $YbBi_4Se_7$ is the aim of the work. These parameters as we know haven't been defined and investigated.

RESULTS AND THEIR DISCUSSION

As it is known the interaction of light with the substance is described by refractive index n and absorption index k which are characterized the phase and damping of plane wave in the substance. These values can be obtained on $R(E)$ by Kramers-Kroning formulae:

$$\theta(E_0) = \frac{E_0}{\pi} \int_0^{\infty} \frac{\ln R(E)}{E_0^2 - E^2} dE . \qquad (1)$$

It is known that the one of material main parameters is its intrinsic energy level, defining the many physicochemical properties, because the material dispersion knowledge allows us to forecast the possibility in principal of definite property realization and its application in semiconductor electronics.

As it is mentioned in [6] the analytical singularities of imaginary part of complex dielectric constant $\varepsilon_2(E)$ and functions connected by state densities dN / dE almost coincide. The band-to-band distance gradient makes the main contribution into dN / dE analytical function singularity:

$$\frac{dN_{ij}}{dE} \sim \int \frac{dS_k}{\left|\nabla_k E_{ij}\right|} ,$$

where $E_{ij}(k)=E_j(k)-E_i(k)$ is distance between conduction and valence bands. The values dN / dE near critic points in k –space defined by $\left|\nabla_k E_{ij}\right|=0$ expression and also the position of critic points and transition type can be theoretically calculated by zone structure.

The analysis of function $\varepsilon_2(E)$, dN / dE and reflection coefficient $R(E)$ show that position in energy spectrum and peak character are similar or very close for these parameters. That's why one can define the values of corresponding band-to-band intervals and band nature with the help of direct comparison of experimental data about curves, crystal reflection in $E>E_g$ region with theoretical calculations of dN / dE function.

As it is mentioned in [6] the state density $N(E)$ is the similar useful notion for crystal and non-crystal substances. By experimental data the state density behavior in non-crystal body not strongly differs from corresponding behavior of crystal state density. The thin structure in first case can be blurred and in forbidden band the local states can appear. The band structure is saved and is defined by short range ordering.

The measurement results of reflection coefficients R(E) and optic function values $YbBi_2Te_4$ and $YbBi_4Se_7$ such as absorption coefficient α, imaginary ε_2 and real ε_1 parts of dielectric constant, absorption index κ and refractive index n, functions of characteristic volume $-\mathrm{Im}(\varepsilon^{-1})$ and surface electron loss $-\mathrm{Im}(1+\varepsilon)^{-1}$, optical conduction function $\varepsilon_2 E$, integral function of bound density of states $\varepsilon_2 E^2$, dielectric constant $\varepsilon_{0,\mathrm{eff}}(E)$, effective number of valence electrons $n_{\mathrm{eff}}(E)$, defined on ε_2, volume $-\mathrm{Im}(\varepsilon^{-1})$ and surface $-\mathrm{Im}(1+\varepsilon)^{-1}$ electron loss, calculated on the base of optical function values $YbBi_2Te_4$ and $YbBi_4Se_7$ participate in transitions up to given energy E [7-11].

The calculated plasma energy E_p for compounds $YbBi_2Te_4$ and $YbBi_4Se_7$ in 8 and 14 free valence electrons is 4,74 and 8,38 eV correspondingly. The calculated resonance frequences 15,1 и 5,9 eV correspondingly [12] are used for comparison of these data with reference ones for other materials, for example, Sb and Na.

The results by parameters: dielectric constants (ε_1,ε_2), electro-optic differential functions (α,β), effective number of valence electrons $n_{\mathrm{eff}}(E)$, defined by volume electron losses $-\mathrm{Im}(\varepsilon^{-1})$ and surface ones $-\mathrm{Im}(1+\varepsilon)^{-1}$ taking part in transitions (on fig.1-5) are presented in the given work.

The measurement results of reflection coefficient spectrum R(E) in materials $YbBi_2Te_4$ and $YbBi_4Se_7$ in beam energy interval 1÷6 eV are given in fig. 1. As it is seen from the figure in case of $YbBi_2Te_4$ if energy increases the reflection coefficient R(E) decreases, and for $YbBi_4Se_7$ R(E) increases and in both cases on curves the peaks which are connected with optic transitions in them, are observed.

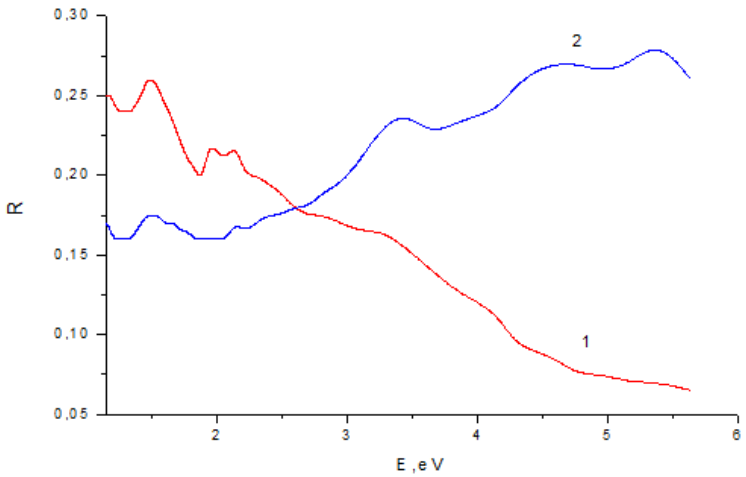

Fig.1. The spectra of reflection coefficients R(E): $YbBi_2Te_4$ (curve 1) and $YbBi_4Se_7$ (curve 2).

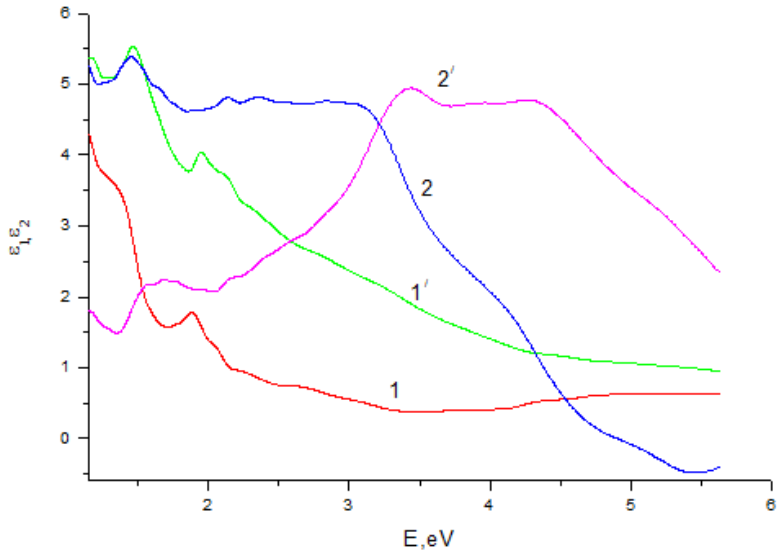

Fig.2. The spectra of dielectric constants ε_1 и ε_2: $YbBi_2Te_4$ (curve 1 and 1′) and $YbBi_4Se_7$ (curve 2 and 2′).

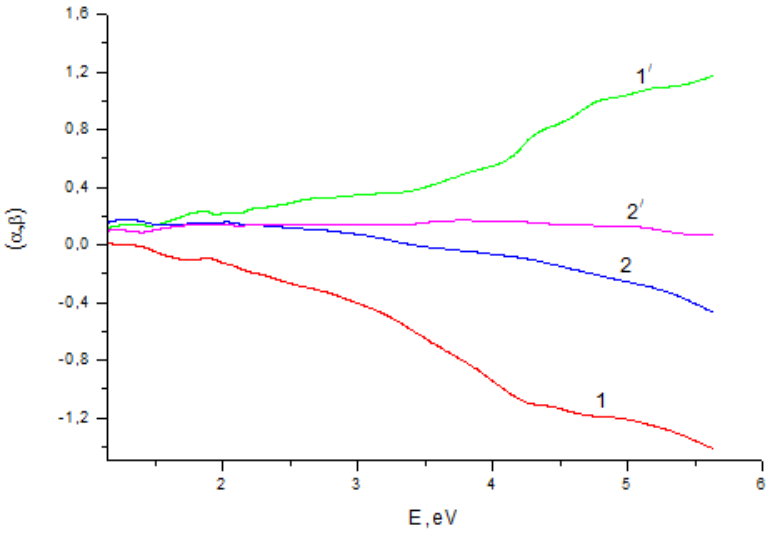

Fig.3. The spectra of electro-optical differential functions (α, β): $YbBi_2Te_4$ (curve 1 and 1') and $YbBi_4Se_7$ (curve 2 and 2').

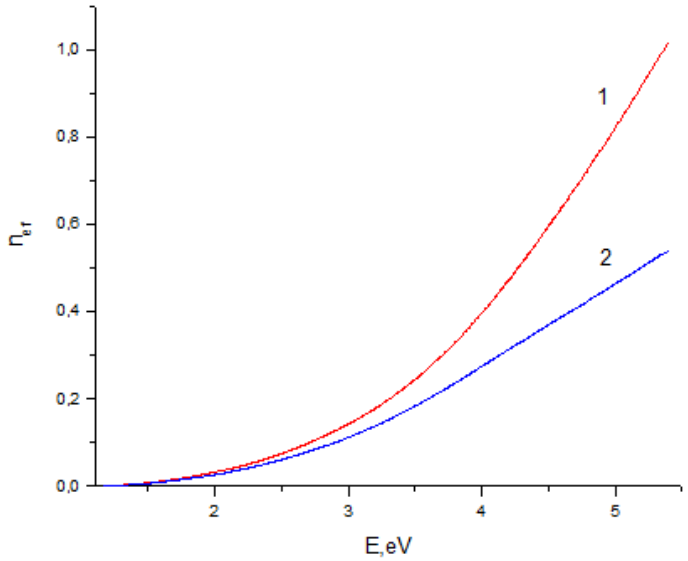

Fig.4. Effective number of valence electrons n_{ef}(E) taking part in transitions up to the given energy *E* by (-Im ε^{-1}) and (-Im$(1+\varepsilon)^{-1}$) for $YbBi_2Te_4$ (curve 1, curve 2).

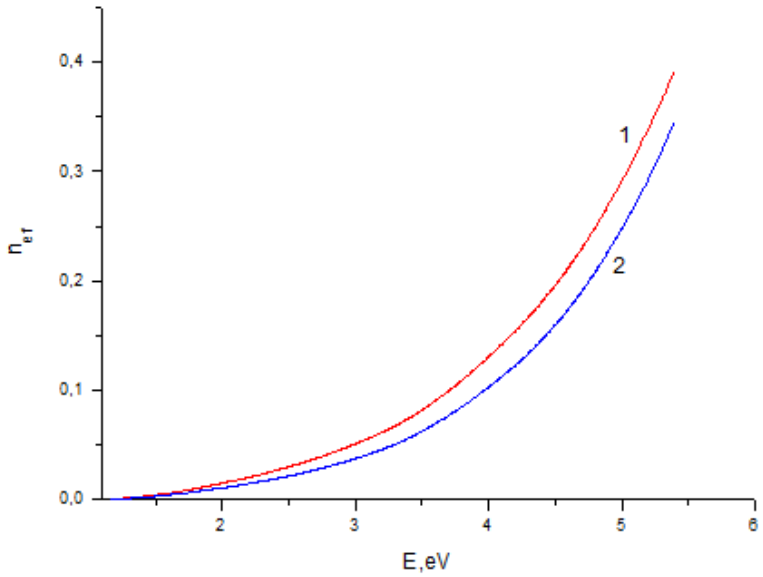

Fig. 5. The effective number of valence electrons n_{ef}(E) taking part in transitions up to the given energy E by (-Im ε^{-1}) and (-Im(1+ ε)$^{-1}$) for $YbBi_4Se_7$ (curve 1, curve 2).

The spectra of dielectric constants of $YbBi_2Te_4$ (curve 1 and 1′) and $YbBi_4Se_7$ (curve 2 and 2′) investigated samples are important material parameters which aren't investigated in scientific literature.

The electro-optical differential functions (α, β) for $YbBi_2Te_4$ (curve 1 and 1') and $YbBi_4Se_7$ (curve 2 and 2') which are defined by absorption k and refraction n coefficients, are presented on fig.3. These parameters play the important role at calculation of material band structure.

The effective number of valence electrons n_{ef}(E) taking part into transitions up to the given energy E by (-Im ε^{-1}) and (-Im(1+ ε)$^{-1}$) $YbBi_2Te_4$ (curve 1, curve 2) and $YbBi_4Se_7$ (curve 1, curve 2), correspondingly are given on fig.4-5. It is seen that in case (-Im ε^{-1}) the number of valence electrons taking part in transitions up to the given energy E is bigger than for case (-Im(1+ ε)$^{-1}$).

As it is seen from fig.1 the reflection coefficients R(E), $YbBi_2Te_4$ (curve 1) и $YbBi_4Se_7$ (curve 2) differ by change character with beam energy behavior. The reflection coefficients R(E) for $YbBi_2Te_4$ (curve 1) with increase of beam energy decreases and for $YbBi_4Se_7$ (curve 2) the increase of reflection coefficient is observed. This can be explained by the difference of their electron structure which generally depends on composition, structure and atomic structure of material component. For $YbBi_2Te_4$ and $YbBi_4Se_7$ the spectrum analogical differences are observed and for their other parameters (fig.2-5).

[1] *Khimiya redkikh elementov. Khalkolantanati redkikh elementov.* (M., Nauka, 1989).(in Rusian)
[2] *T.F. Maksudova*. Fiziko-khimicheskie osnovi polucheniya troynikh soedineniy v sistemakh Eu(Yb)-Sb(Bi)-X (X=S, Se, Te). Avtoref. Diss. dok. khim. nauk (Baku 2005). (in Rusian)
[3] *P.G. Rustamov, T.F. Maksudova, O.M. Aliyev*. Kishinyov, ShTIINTsA (1983) s.45. (in Rusian)
[4] *O.M. Aliyev*. Fiziko-khimicheskie osnovi polucheniya troynikh poluprovodnikovikh faz, proizvodnoy strukturi Yb_3S_4 и Y_5S_7. Avtoref. Diss. dok. khim. nauk (Sverdlovsk, IKh UNTsAN SSSR, 1985). (in Rusian)
[5] *O.M. Aliyev, T.F. Maksudova, N.D. Samsonova, L.D. Finkelshteyn, P.G. Rustamov*. Neorgan. materiali, 22, 29 (1986). (in Russian)
[6] *K.K. Shvarts, Yu.N. Shunin, Ya.A. Teteris*. Izv. AN Lat. SSR, ser. fiz. i tekh. nauk, n.4, 51 (1987). (in Russian)
[7] *N.Z. Jalilov, G.M. Damirov.* FTP, 45, 1223 (2011). (in Russian)
[8] *N.Z. Jalilov, G.M. Damirov.* FTP, 45, 500 (2011). (in Russian)
[9] N.Z. Jalilov, M.A. Makhmudova. Izv. NAN Azerb., ser. fiz.-mat. i tekhn., fiz i astr., XXVIII, n.5, 71 (2010). (in Russian)
[10] *N.Z. Jalilov, M.A. Makhmudova, G.M. Damirov.* «Sovremennie problem nanoelektroniki, nanotekhnologiy, mikro- i nanosistem». Ulyanovsk, 2010, s.31. (in Russian)
[11] *N. Mott, E. Devis.* Elektronnie protsesi v nekristallicheskikh veshestvakh (M., Mir, 1982).(in Russian)
[12] *F. Platsman, P. Volf.* Volni i vzaimodeystviya v plazme tverdogo tela (M., Mir, 1975).(in Russian)

Received: 23.05 2013

ISSN 1028-8546

2013, Vol. XIX, № 3
Section: En

CONTENTS